J. Fluid Mech. (1981), *vol.* 113, *pp.* 433-467
Printed in Great Britain

The development of a turbulent wake in a distorting duct

By C. J. ELLIOTT
Trinity Hall, Cambridge
AND A. A. TOWNSEND
Emmanuel College, Cambridge

(Received 7 October 1980 and in revised form 13 March 1981)

Characteristics of the turbulent motion in a cylinder wake have been measured during passage through a distorting section of a wind tunnel, the overall effect of the distortion being considerable lateral extension and compression without a considerable change of flow velocity. However, the sectional area is not constant and rates of longitudinal extension are comparable with the rates of lateral straining. Hot-wire anemometers, mostly in X-configurations, are used to measure mean velocities, turbulent intensities, Reynolds stresses, intermittency factors and spectra, and velocity correlations have been calculated from digital recordings of the outputs from arrays of eight single-wire anemometers. In contrast to previous investigations, the direction of compression is parallel to the axis of the cylinder, and the original entrainment eddies of the plane wake are suppressed rather than amplified.

The results show that substantial changes in stress-intensity ratios, entrainment rates, dissipation rates and turbulence length-scales occur in response to the three-dimensional distortion. In particular, the ratio of Reynolds stress to total intensity increases during the initial acceleration of the flow before decreasing as the flow is strained laterally, and correlations show that length-scales do not change in proportion to the lateral extension and become relatively small compared to the flow width.

1. Introduction

For the understanding of turbulent shear flow, a central problem is the interaction between the turbulent motion and the gradients of mean velocity. If the mean flow is effectively unidirectional, as in many jets, wakes and boundary layers, distortion of the turbulence is almost entirely by a simple shearing and the components of the Reynolds-stress tensor have much the same ratios in all the flows. More complex modes of distortion appear if the streamlines of the mean flow are appreciably divergent or curved, and they lead to considerable changes in the turbulent motion, not only in the stress ratios but in length scales, eddy geometry and rates of entrainment.

One flow with complex distortion of the turbulence is a turbulent wake developing as it passes through a distorting duct with sections of constant area but changing aspect ratio. In addition to the 'normal' simple shearing, the turbulence experiences irrotational extension and compression in the plane at right angles to the flow, and the consequent enhancement and alignment of vorticity in the direction of extension leads to modification of flow geometry and flow processes. Reynolds (1962) and Keffer

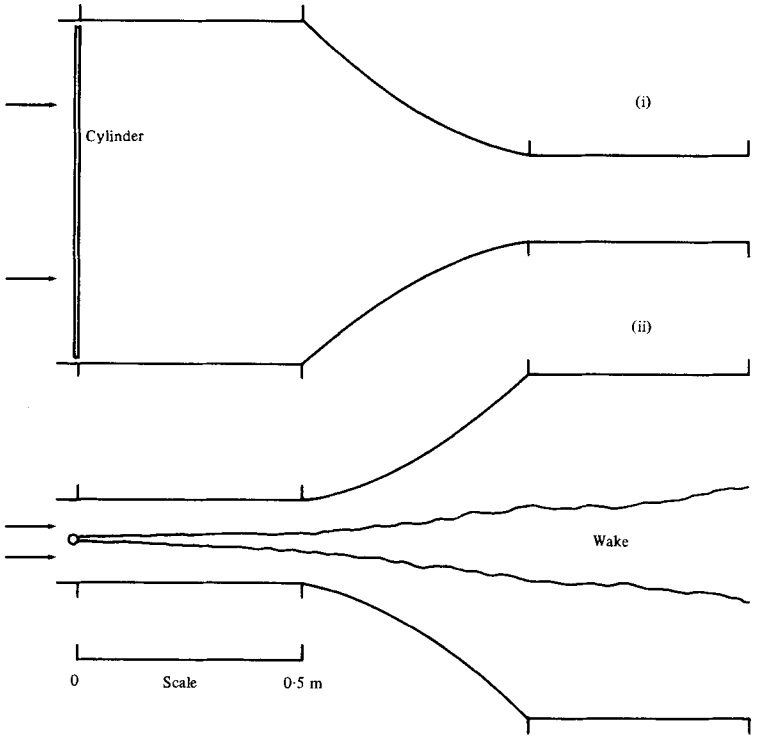

FIGURE 1. Longitudinal sections of the distorting duct.

(1965, 1967) have studied wake turbulence in a constant-area duct with height varying exponentially with distance from the entrance, the direction of compression being at right angles to the plane of the wake. For that direction of compression, large increases in rate of entrainment of ambient fluid occur as entrainment eddies with axes parallel to the direction of extension gain energy from the irrotational flow, and there are changes in the stress ratios and in the spectra of the velocity fluctuations. In the flow with the direction of extension at right angles to the plane of the wake, entrainment eddies are expected to lose energy to the irrotational flow with consequent reduction in rate of entrainment. An interesting question is whether the wake develops an alternative mechanism of entrainment that is not inhibited by the lateral straining. The experimental work to be described includes measurements of distributions of mean velocity defect and turbulent intensities, of mean-square velocity derivatives, of intermittency factors, and of velocity spectra and correlations, and one purpose was to find if the measured changes in stress-intensity ratios and correlation functions could be described by an application of the rapid-distortion approximation to the equations of motion (Elliott 1976; Townsend 1980). Here, the measurements are analysed to provide information also about overall properties of the flow such as entrainment rates, rates of energy dissipation, profile shapes and eddy length scales, as well as local properties such as the stress-intensity ratios.

2. Experimental arrangements

The layout of the tunnel working section is sketched in figure 1. The flow passes first through a parallel section of length 0·51 m and lateral dimensions $0{\cdot}19 \times 0{\cdot}76\,\mathrm{m}^2$ (horizontal to vertical) before entering a distorting section of similar length over which the section changes to $0{\cdot}76 \times 0{\cdot}19\,\mathrm{m}^2$. The recovery section is parallel-sided and exhausts into the room. The wake was produced by a cylindrical rod of diameter 3·18 mm, spanning the tunnel entrance with its axis vertical.

Airflow velocities past the cylinder were not exactly the same for all runs, but no systematic dependence of the non-dimensional quantities on flow velocity could be seen. For the data described here, the average flow velocity was $8{\cdot}45\,\mathrm{m\,s^{-1}}$, and the cylinder Reynolds number was 1780. The entrance to the distorting section is 160 diameters distant from the cylinder and, in a parallel free stream, the development of the wake would be nearly self-preserving (Townsend 1949).

Mean velocities and turbulent intensities were measured using hot-wire anemometers with two wires arranged in the form of an 'X', each at an angle of roughly 45° to the support. Each was connected in a conventional, constant-resistance control bridge, and the response is thought to be substantially uniform from 0·5 Hz to at least 5 kHz. They were calibrated statically, either *in situ* with the cylinder removed or in a separate wind tunnel, by measuring the bridge output for a range of flow velocities and directions, typically for a range of 2·5 : 1 in velocity and 30° in angle. The calibration data for each wire was fitted to the relation

$$E^2 = a + bU_e^{\frac{1}{2}}, \tag{2.1}$$

in which

$$U_e^2 = U^2(\cos^2(\theta-\phi) + \alpha\sin^2(\theta-\phi))$$

where E is the output voltage, U is the flow velocity, θ is the angle between the flow direction and the probe support; a, b, ϕ, α are chosen for best fit to the data.

In use, mean output voltages are measured for each wire, and the mean velocity and direction found by solving equation (2.1). If the flow direction lies within the range of calibration, the incremental sensitivities to cross-stream and streamwise fluctuations are easily calculated. The fluctuations of the output voltages, e_a and e_b, were amplified and mean values of e_a^2, e_b^2, $(e_a+e_b)^2$ and $(e_a-e_b)^2$, were obtained using analogue circuits for adding and squaring and resistance capacity filters with time constants of about 10 s.

For measurements of intensities, Reynolds stresses, mean velocity and intermittency, the hot-wire probe was moved across the wake in steps and, at a suitable interval after each movement, the mean bridge voltages, the mean squares and the probe position were recorded in digital form on paper tape. The interval between steps was approximately 35 s.

Spectra were obtained from digital recordings of the anemometer outputs, sampled at intervals of 0·256 ms. Standard methods used fast Fourier transform routines to calculate the power spectra of the velocity components and their cross-spectrum.

Information about flow patterns of the turbulent motion was derived from digital recordings from arrays of eight single-wire anemometers, arranged at intervals of 10 mm in a line and with the outputs sampled at intervals of 1·024 ms. The recorded data were analysed to give time-delay cross-correlations for all the sensor pairs.

3. Flow equations

The flow is described with respect to rectangular axes with Oy the axis of the cylinder and Ox the centre-line of the tunnel. Components of the mean velocity are U, V, W, and the components of the velocity fluctuation are u, v, w.† Since the flow is essentially incompressible, pressures and stresses take their kinematic forms.

The proper way to describe the flow change induced by the wake is by changes along the streamlines of the mean flow, but the wake causes such small lateral displacements of the streamlines (at most 1·6 mm) that it is sufficiently accurate to use changes at fixed points. At 160 diameters from the cylinder, the changes in the lateral component of mean velocity are less than changes in the longitudinal components in a ratio of nearly l_0/x, where l_0 is the width scale of the wake defined by

$$l_0^2 = \int (U_1 - U) z^2 \, dz \Big/ \int (U_1 - U) \, dz,$$

the suffix 1 denoting a value in the absence of the cylinder.‡ Since the ratio is approximately 0·02 at 160 diameters, the lateral component of mean velocity in the wake flow can be set equal to that in the basic flow without appreciable error.

Then the equation for the cross-stream component of mean velocity on the central plane, $y = 0$, is

$$U\frac{\partial W_1}{\partial x} + W_1\frac{\partial W_1}{\partial z} + \frac{\partial \overline{uw}}{\partial x} + \frac{\partial \overline{w^2}}{\partial z} = -\frac{\partial P}{\partial z},$$

or, subtracting the equation for the basic flow,

$$(U - U_1)\frac{\partial W_1}{\partial x} + \frac{\partial \overline{uw}}{\partial x} + \frac{\partial \overline{w^2}}{\partial z} = -\frac{\partial}{\partial z}(P - P_1), \tag{3.1}$$

where P_1 and P are the mean pressures in the basic and wake flows. The change in mean velocity on the centre-line is nearly $u_0 = U_1/(x/d)^{\frac{1}{2}} \simeq 5U_1 l_0/x$ (d is the cylinder diameter), and so the first two terms are of order u_0^2/x and so small compared with the third. Since $P = P_1$ outside the wake,

$$P - P_1 + \overline{w^2} = 0. \tag{3.2}$$

The equation for the longitudinal component is

$$U\frac{\partial U}{\partial x} + W_1\frac{\partial U}{\partial z} + \frac{\partial \overline{u^2}}{\partial x} + \frac{\partial \overline{uw}}{\partial z} = -\frac{\partial P}{\partial x},$$

and, by subtracting the equation for the basic flow, it may be transformed to

$$\left(U\frac{\partial}{\partial x} + W_1\frac{\partial}{\partial z}\right)(U - U_1) + \frac{\partial}{\partial x}(\overline{u^2} - \overline{w^2}) + \frac{\partial \overline{uw}}{\partial z} + \frac{\partial U_1}{\partial x}(U - U_1) = 0. \tag{3.3}$$

Using the condition of incompressibility, equation (3.3) can be integrated across the flow to give an equation for the momentum integral,

$$\frac{d}{dx}\int U(U - U_1)\, dz + \frac{\partial V_1}{\partial y}\int (U - U_1)\, dz + \frac{dU_1}{dx}\int (U - U_1)\, dz = 0. \tag{3.4}$$

† At times, it is convenient to use tensor notation when the axial directions Ox, Oy, Oz correspond with suffixes 1, 2, 3.

‡ Throughout, the range of integrals is to be understood as the complete width of the wake.

Here, V has been put equal to V_1 and is assumed to be independent of z, and a term $(d/dx)\int(\overline{u^2}-\overline{w^2})dz$ has been omitted as being small compared with the terms retained.

Putting $\partial V_1/\partial y = (U_1/b)\,db/dx$, where b is the extension ratio of the flow in the Oy direction near the centre-line,

$$\frac{d}{dx}\left[U_1^2 b\int(U-U_1)\,dz\right]+U_1 b\frac{d}{dx}\int(U-U_1)^2\,dz=0, \tag{3.5}$$

and, if $|U-U_1|\ll U_1$,

$$U_1^2 b\int(U-U_1)\,dz = M \text{ (a constant)}. \tag{3.6}$$

The equation for the total turbulent kinetic energy, $\frac{1}{2}\overline{q^2}$ (where $q^2=u^2+v^2+w^2$), is

$$(U\,\partial/\partial x+W\,\partial/\partial z)\,\tfrac{1}{2}\overline{q^2}+\partial/\partial z(\overline{pw}+\tfrac{1}{2}\overline{q^2}w)$$
$$+\overline{u^2}\,\partial U/\partial x+\overline{v^2}\,\partial V/\partial y+\overline{w^2}\,\partial W/\partial z+\overline{uw}\,\partial U/\partial z+\epsilon=0, \tag{3.7}$$

where ϵ is the local rate of turbulent energy dissipation. Integrating across the wake gives

$$\frac{1}{b}\frac{d}{dx}\left[U_1 b\int\tfrac{1}{2}\overline{q^2}\,dz\right]+\int(\overline{u^2}\,\partial U/\partial x+\overline{v^2}\,\partial V/\partial y+\overline{w^2}\,\partial W/\partial z)\,dz$$
$$+\int\overline{uw}\,(\partial U/\partial z)\,dz+\int\epsilon\,dz=0, \tag{3.8}$$

omitting the small term $(d/dx)\int\frac{1}{2}\overline{q^2}(U-U_1)\,dz$. All the terms can be calculated from the measurements except the total dissipation. To distinguish between energy production by working of the normal stresses against longitudinal gradients of mean velocity and production by the lateral straining, the integrand of the second term may be rewritten as

$$\overline{u^2}\,\partial U/\partial x+\overline{v^2}\,\partial V/\partial y+\overline{w^2}\,\partial W/\partial z$$
$$=(\overline{u^2}-\tfrac{1}{2}(\overline{v^2}+\overline{w^2}))\,\partial U/\partial x+\tfrac{1}{2}(\overline{v^2}-\overline{w^2})\,(\partial V/\partial y-\partial W/\partial z). \tag{3.9}$$

The rate of entrainment of non-turbulent ambient fluid into the wake can be found from the intermittency signal $\delta(\mathbf{x},t)$, defined to be zero in non-turbulent fluid and one in turbulent fluid. The flux of turbulent fluid is $(\mathbf{U}+\mathbf{u})\,\delta$, and so the local rate of conversion of ambient to turbulent fluid is

$$\operatorname{div}[(\mathbf{U}+\mathbf{u})\,\delta]=U\,\partial\delta/\partial x+V\,\partial\delta/\partial y+W\,\partial\delta/\partial z+\partial(u\delta)/\partial x+\partial(v\delta)/\partial y+\partial(w\delta)/\partial z. \tag{3.10}$$

Averaging and then integrating over the width of the wake, the mean rate of conversion per unit area in the xOy plane is

$$2u_e=\frac{d}{dx}\int\overline{(U+u)\,\delta}\,dz+\int\frac{\partial}{\partial y}[\overline{(V+v)\,\delta}]\,dz \tag{3.11}$$

or, to the approximation that $|U_1-U|\ll U_1$,

$$u_e=d(U_1\eta_0)/dx+\eta_0\,\partial V_1/\partial y, \tag{3.12}$$

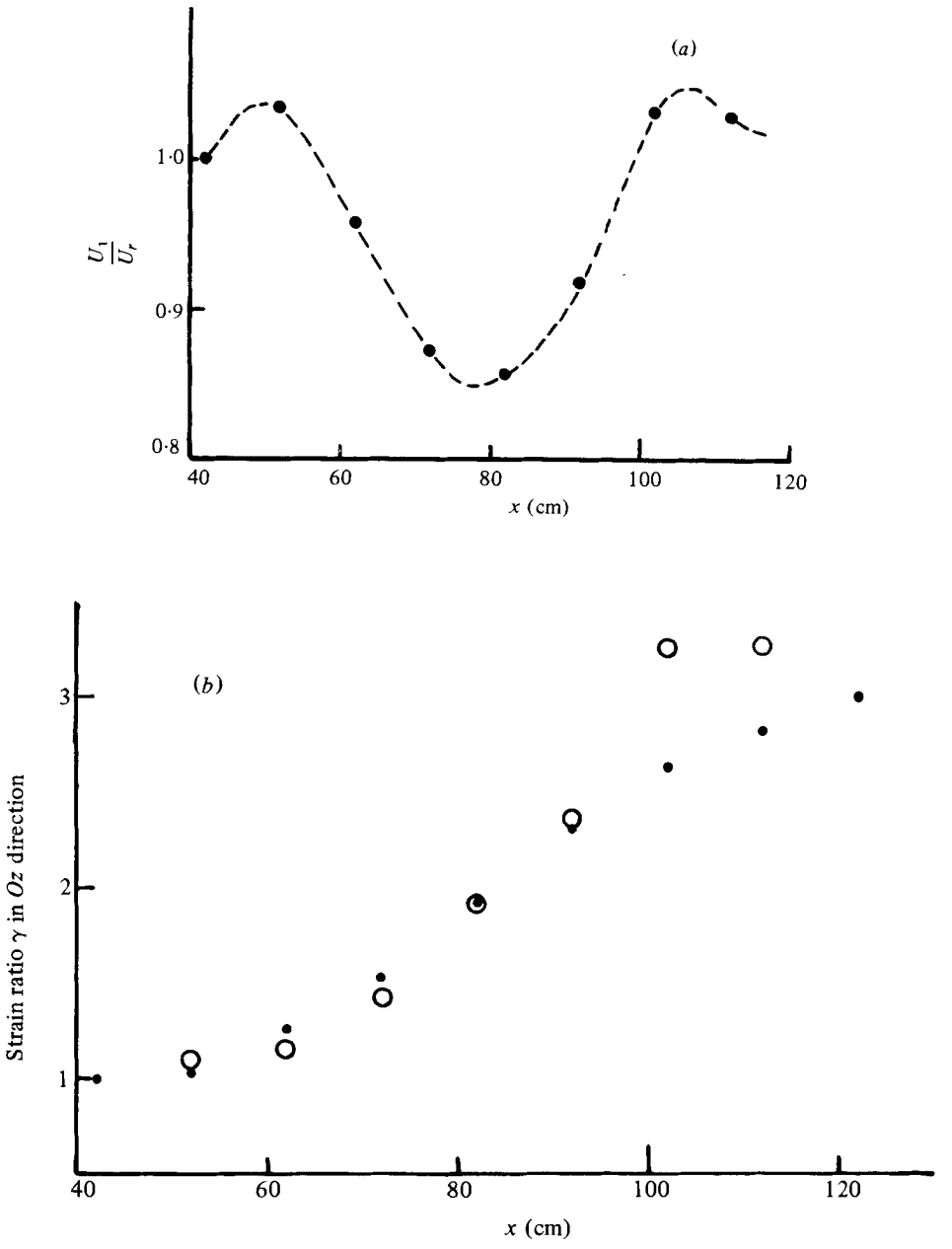

FIGURE 2. (*a*) Variation of flow velocity on the centre-line in the absence of the cylinder. (*b*) Variation of strain ratio in the Oz direction. ●, Calculated from measured angles of flow; ○, calculated assuming $M = U_1^2 b \int (U_1 - U)\,dz$ is constant.

where $2\eta_0 = \int \bar{\delta}\,dz$. Putting $\partial V_1/\partial y = (U_1/b)\,db/dx$ as before,

$$u_e = b^{-1} d(U_1 b \eta_0)/dx \tag{3.13}$$

defined as the entrainment velocity across the bounding surface of the wake.

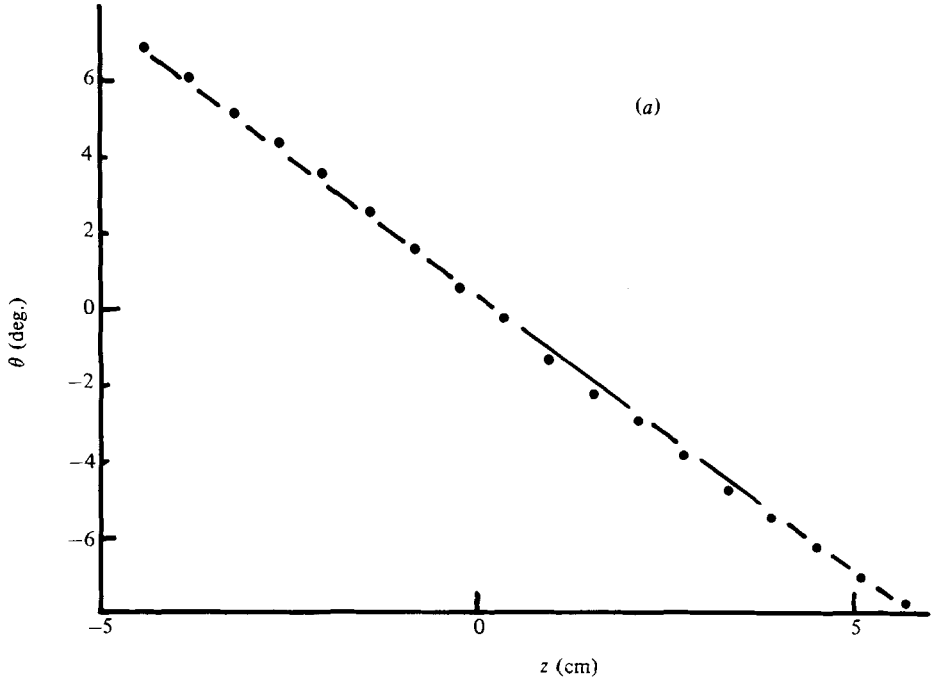

FIGURE 3(*a*). For legend see page 440.

4. Mean velocity distributions

Because the transitions between the parallel flow sections and the distorting section are very abrupt, considerable flow separation occurs in the internal angles, at the top and bottom at entrance to the distortion and at the side walls on exit. Consequently, it is not possible to calculate the basic flow from the duct dimensions and the velocity distribution must be found by measurement.

Figure 2 shows the measured distribution of mean velocity close to the duct axis, expressed as a ratio to U_r, the velocity on the axis at the reference position $x_r = 0{\cdot}42$ m. The ratio, $U_1/U_r = a$, is the extension ratio in the stream direction between the reference position and the position of measurement. The results are derived both from measurements with X-wires and with linear arrays of hot-wires aligned normal to the flow direction. No significant inhomogeneity in the Oy direction was found.

The lateral extension ratios were obtained from the measurements of flow direction in traverses of X-wires across the wake. Within the uncertainty of measurement, the angle between the flow direction and the tunnel axis, θ, is a linear function of displacement in the Oz direction (figure 3a, b). Since the angles are small, $\tan\theta = W/U$ is nearly equal to θ, and the slope is

$$\frac{\partial\theta}{\partial z} = \frac{1}{U}\frac{\partial W}{\partial z}. \tag{4.1}$$

The velocity defects are small and the average slopes of the θ–z plots is a good approximation to $U_1^{-1}\partial W_1/\partial z$, where $\partial W_1/\partial z$ is the rate of lateral extension in the Oz direction.

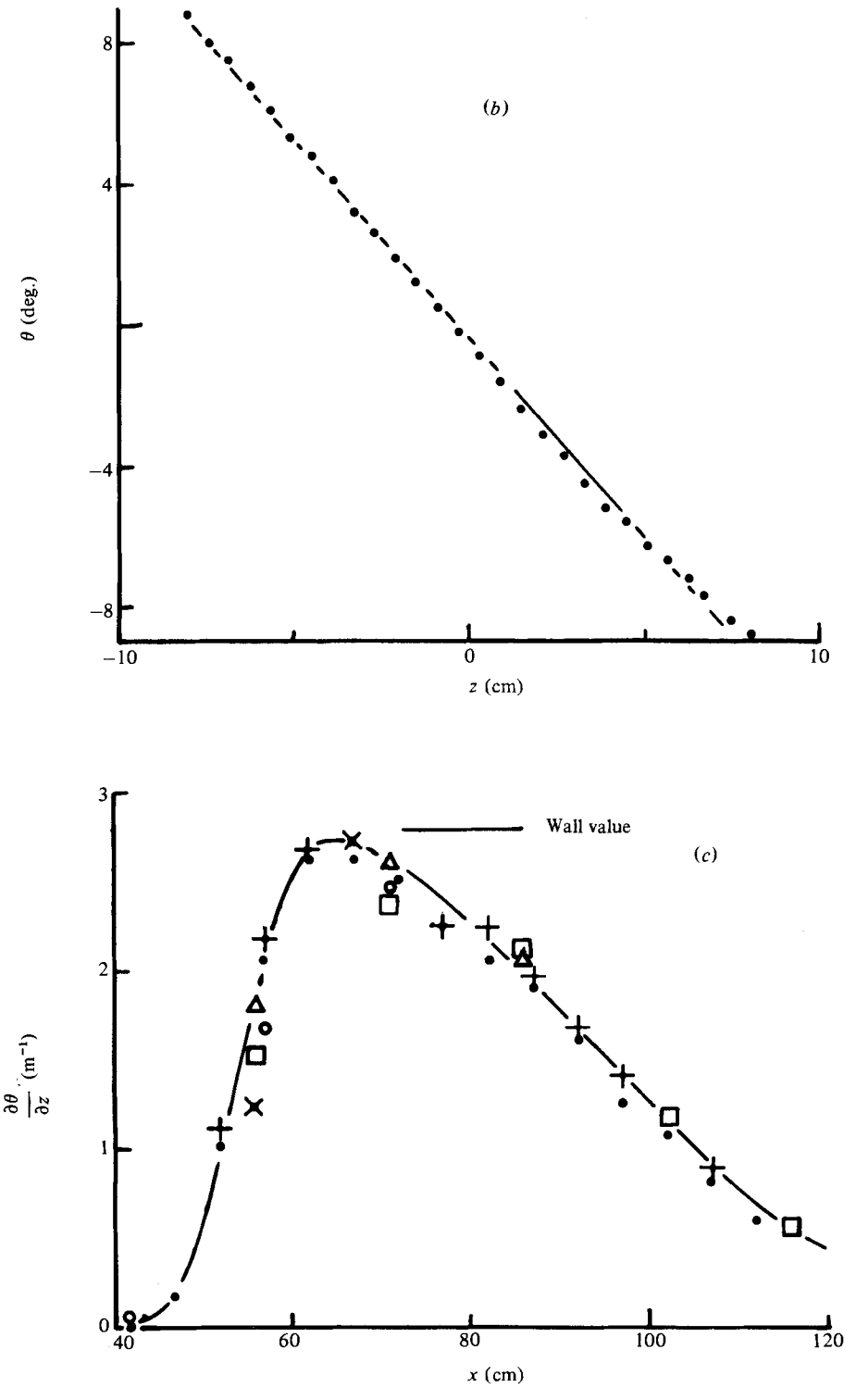

FIGURE 3. Angles of inclination of the mean flow. (*a*) Lateral variation for $x = 72$ cm. (*b*) Lateral variation for $x = 82$ cm. (*c*) Divergence rate against downstream distance.

Then, by numerical integration of the slope measurements (figure 3*c*), the total strain of the basic flow from the reference position can be found as

$$c = \int_{x_r} \frac{1}{U_1} \frac{\partial W_1}{\partial z} dx = \int_{x_1} \frac{\partial \theta}{\partial z} dx. \tag{4.2}$$

Figure 2(*b*) shows values of the lateral strain c found in this way, together with values obtained by assuming invariance of the momentum perameter defined by equation (3.6). The two sets of values are in fair agreement for distances from the cylinder less than 1 m. The occurrence of flow separation is responsible for the difference between the final extension ratio of nearly three and the wall separation ratio of four.

Mean velocities in the wake have been obtained from traverses with X-wires, with linear arrays of single wires and with total head tubes. The distributions of velocity defect are similar in shape to the Gaussian error function, the main difference being a more rapid approach to the free-stream velocity (figure 4). Since the shapes are all so nearly the same, the distributions may be specified by a length scale, l_0, and a velocity scale, u_0, defined by

$$l_0^2 = \int (U_1 - U) z^2 dz \Big/ \int (U_1 - U) dz \tag{4.3}$$

and by

$$u_0 = \int (U_1 - U) dz \times (\sqrt{[2\pi]}\, l_0)^{-1}. \tag{4.4}$$

If the distributions were precisely error functions, the velocity scale would equal the maximum velocity defect. Using data from traverses of the linear array, values of the scales were found and shown in table 1 and plotted in figure 5.

To test the assumption that the wake flow is essentially homogeneous in the *Oy* direction, the momentum parameter (M of equation (3.6)) has been calculated from the array measurements with results shown in figure 6. For distances from the cylinder less than 1 m, no significant variation is to be seen but it then begins to increase. The increase is almost certainly caused by transfer of momentum between the wake and the boundary layers on the top and bottom of the duct. It may be noticed that the overall width of the wake at $x = 1$ m is 80 mm, compared with the duct height of 190 mm.

5. Distributions of turbulent intensity and Reynolds stress

Lateral distributions of the three components of turbulent intensity and of the Reynolds stress have been obtained from traverses at distances from the cylinder in the range 41–116 cm, and the distributions from one sequence of traverses are shown in non-dimensional form in figure 7. The intensity scales are the central values or, for the Reynolds stress, the maximum absolute value, and the length scale is l_0 as defined by equation (4.3). Excepting the distributions of $\overline{w^2}$, the shapes change little during passage through the distortion and scales of intensity and width are sufficient to describe the changes. The change in shape of the distributions of $\overline{w^2}$ is considerable (compare figures 7*e*,*f*). Upstream of the distorting section, the shape is similar to that

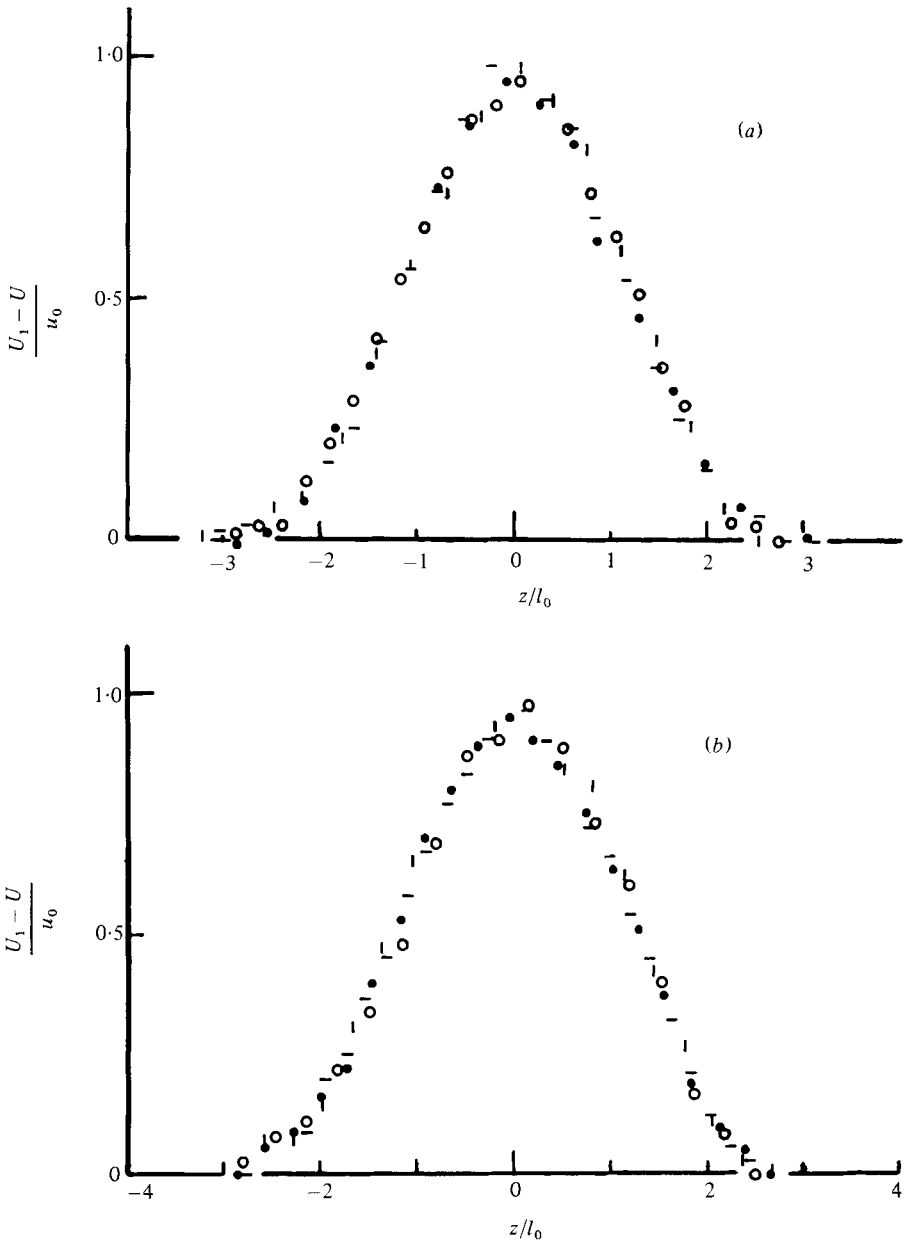

FIGURE 4. Non-dimensional distributions of velocity defect. (*a*) ●, x = 42 cm; ——, x = 52 cm; ○, x = 62 cm; |, x = 72 cm. (*b*) ●, x = 82 cm; ——, x = 92 cm; ○, x = 102 cm; |, x = 112 cm.

found in a uniform stream with a central maximum, but distributions towards the end of the distortion have developed a central minimum and subsidiary maxima.

Scales of intensity and width for the distributions are plotted in figures 8 and 9 and are listed in table 2. The width scales for the three components, L_1, L_2, L_3 respectively, are half the separation of the positions where the intensity is one-half of the central value, and they are plotted as ratios to the mean velocity length scale l_0. Qualitatively, the ratios for all three components change in similar ways with distance downstream,

x	$a = U_1/U_r$	b	c	l_0 (cm)	u_0/U_r
42	1·000	1·000	1·000	0·855	$7{\cdot}2 \times 10^{-2}$
52	1·035	0·895	1·08	1·065	$5{\cdot}8 \times 10^{-2}$
62	0·978	0·825	1·24	1·215	$6{\cdot}0 \times 10^{-2}$
72	0·873	0·750	1·53	1·657	$6{\cdot}1 \times 10^{-2}$
82	0·857	0·604	1·93	2·163	$6{\cdot}2 \times 10^{-2}$
92	0·919	0·467	2·33	2·834	$5{\cdot}5 \times 10^{-2}$
102	1·031	0·367	2·64	3·578	$5{\cdot}4 \times 10^{-2}$
112	1·029	0·345	2·82	4·214	$4{\cdot}7 \times 10^{-2}$

TABLE 1. Parameters of the mean velocity field.

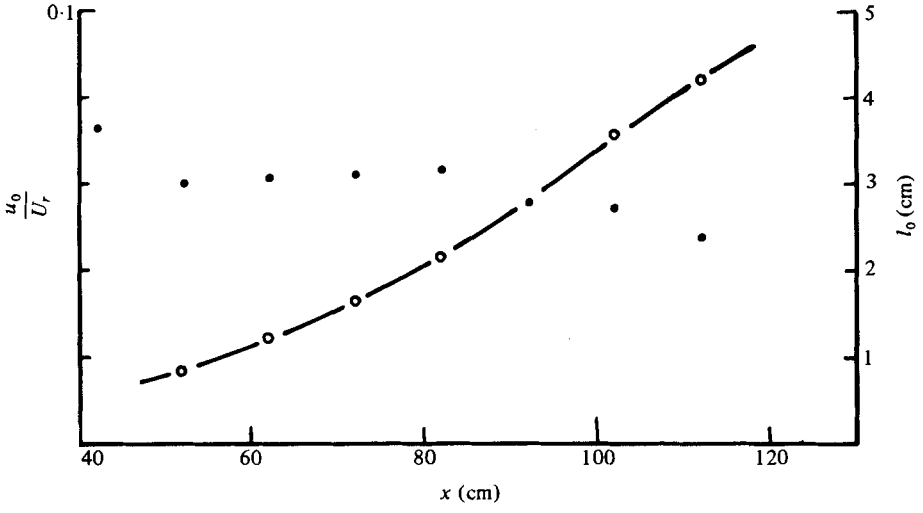

FIGURE 5. Magnitudes of mean velocity scale and flow width scale. ●, velocity scale as ratio to reference velocity; ○, flow width scale.

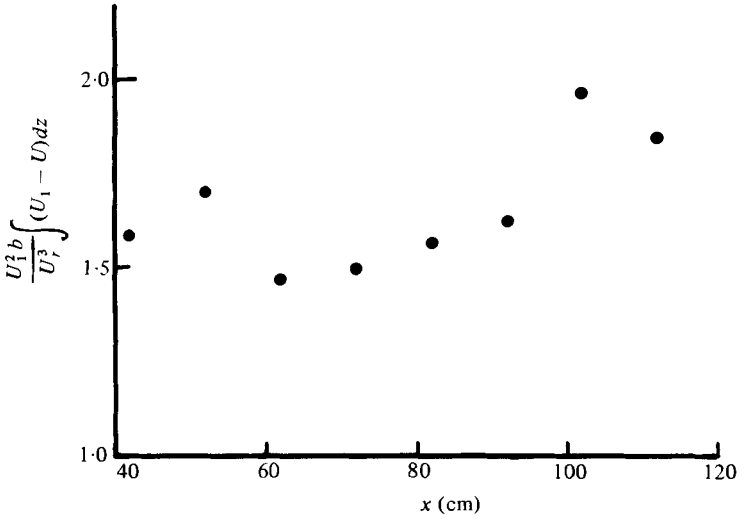

FIGURE 6. Variation of the momentum integral of equation (3.6).

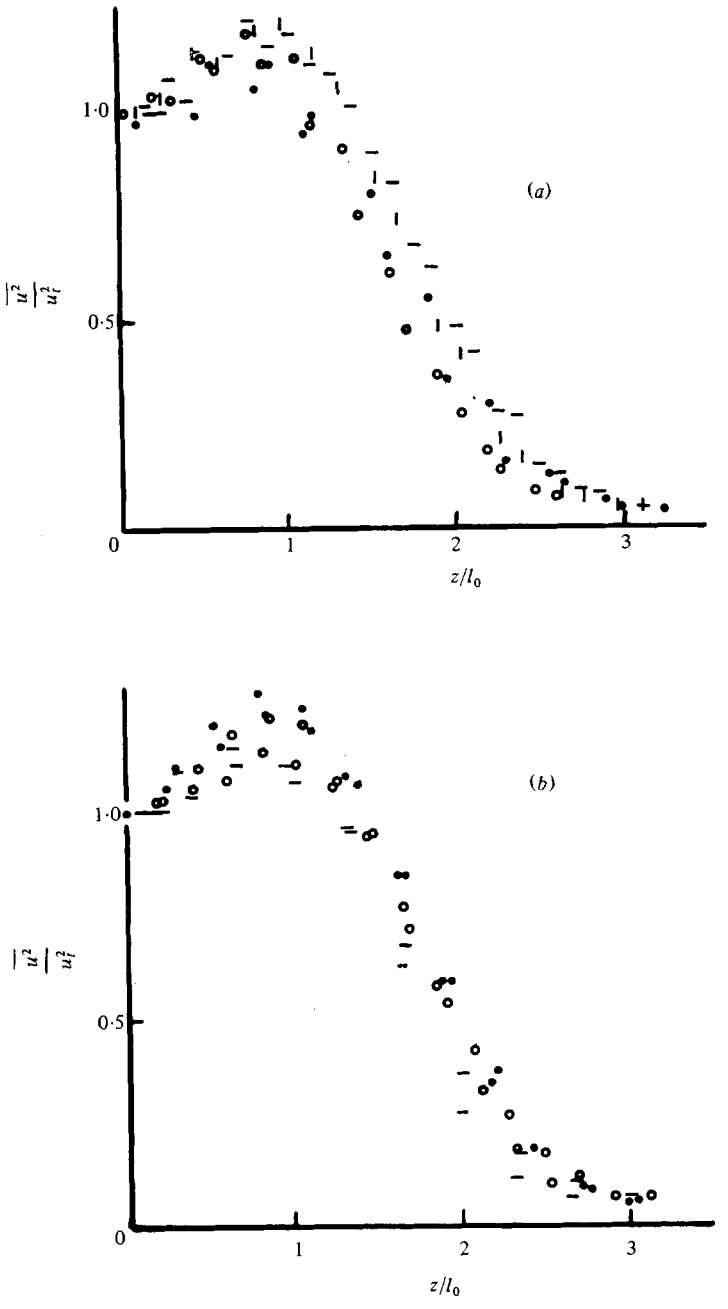

FIGURE 7(a, b). For legend see page 447.

with an initial decrease between $x = 41$ cm and $x = 56$ cm followed by an increase to maximum values near $x = 80$ cm and a return to nearly the initial values beyond $x = 1$ m. The changes are greatest for the distributions of $\overline{w^2}$ and least for the distributions of $\overline{v^2}$.

Ratios of intensities and Reynolds stress to the total turbulent intensity, $\overline{q^2} = \overline{u^2} + \overline{v^2} + \overline{w^2}$, appear in many predictive theories of turbulent flow. The ratios of

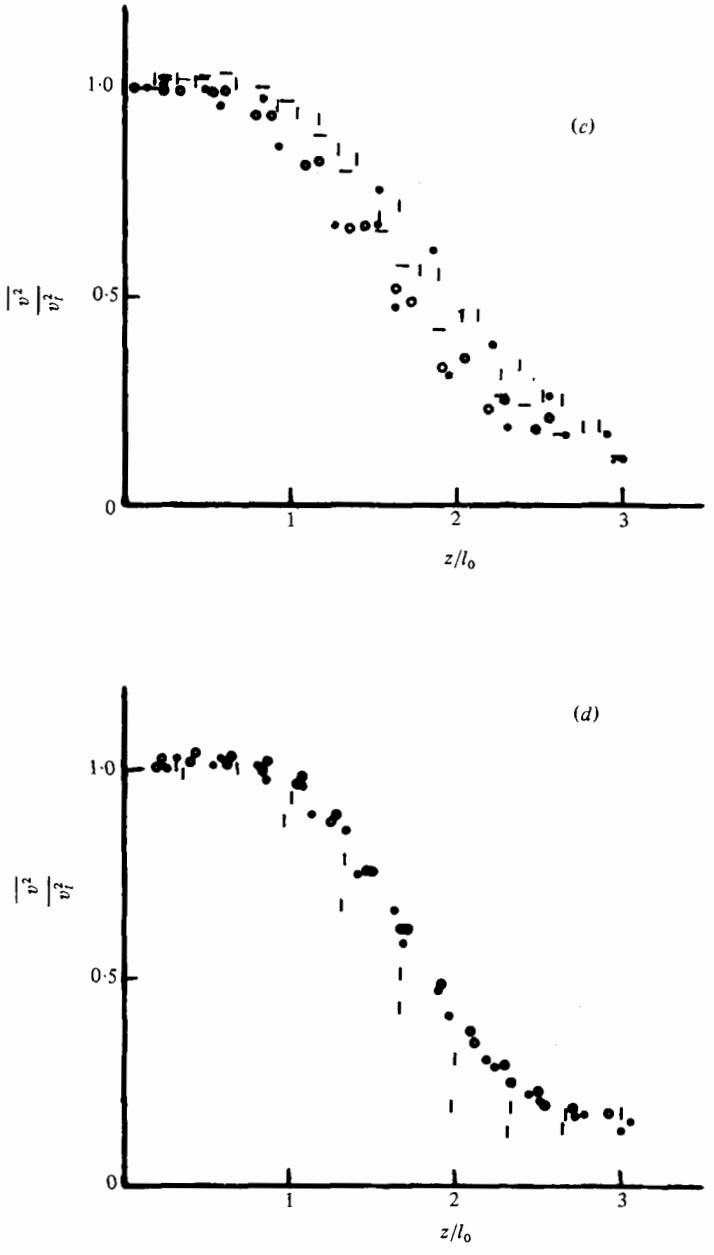

FIGURE 7 (*c*, *d*). For legend see page 447.

the three intensities on the central plane change with downstream distance in much the same way as do the ratios for grid turbulence passing through a similar duct (Tucker & Reynolds 1968), with the coefficient of lateral anisotropy, $(\overline{v^2}-\overline{w^2})/(\overline{v^2}+\overline{w^2})$ reaching a value of 0·50 at $x = 102$ cm. The stress-intensity ratio, $a_1 = |\overline{uw}|/\overline{q^2}$, measured near the position of maximum shear stress and velocity gradient, increases from a value near 0·16 at $x = 41$ cm to a maximum value of perhaps 0·19 at $x = 51$ cm, the entrance to the distortion and a position of maximum flow velocity. Thereafter, the ratio decreases steadily to around 0·11 at exit from the distortion.

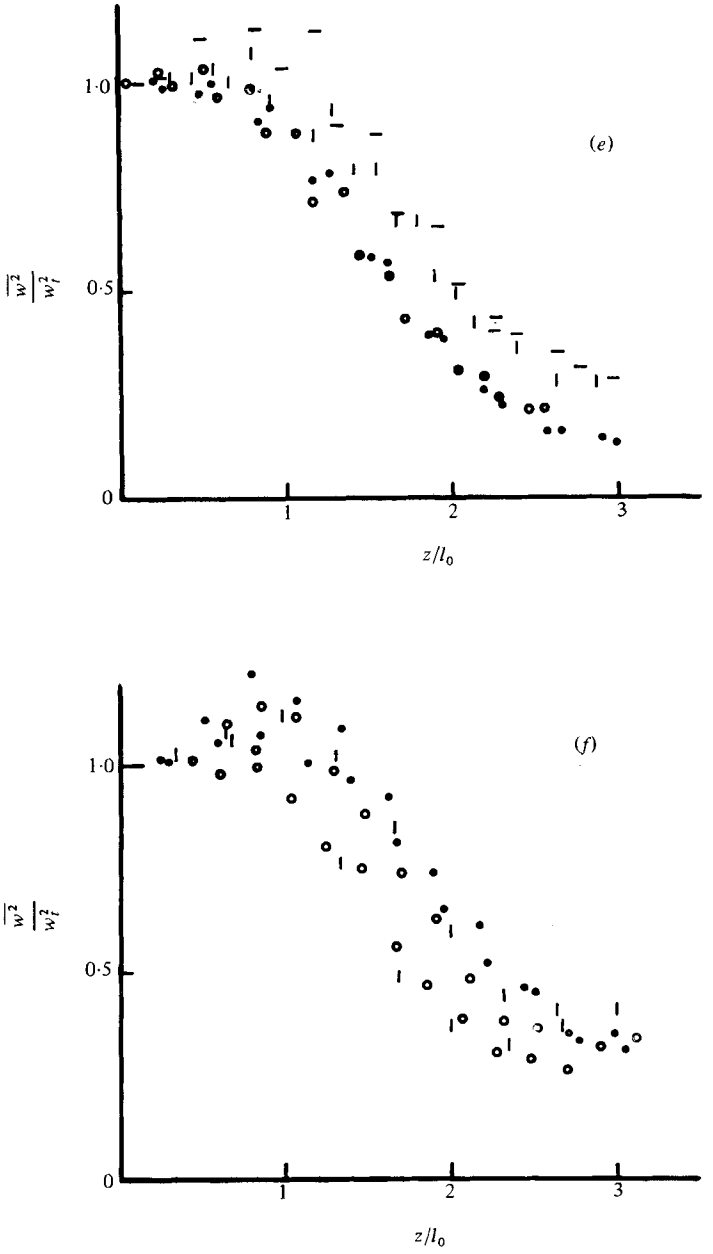

FIGURE 7 (*e*, *f*). For legend see page 447.

From records of traverses with the plane of the X-wire parallel to the cylinder axis, values of the transverse Reynolds stress, $-\overline{uv}$, were calculated and were found to be distributed asymmetrically with maximum values up to one-third of the maximum value of the shear stress. During these traverses, the direction of mean flow could be at a considerable angle to the plane of the X-wire, and small misalignments of the wires may generate fictitious values of the transverse stress. In fact, runs with different hot-wire assemblies gave very different values.

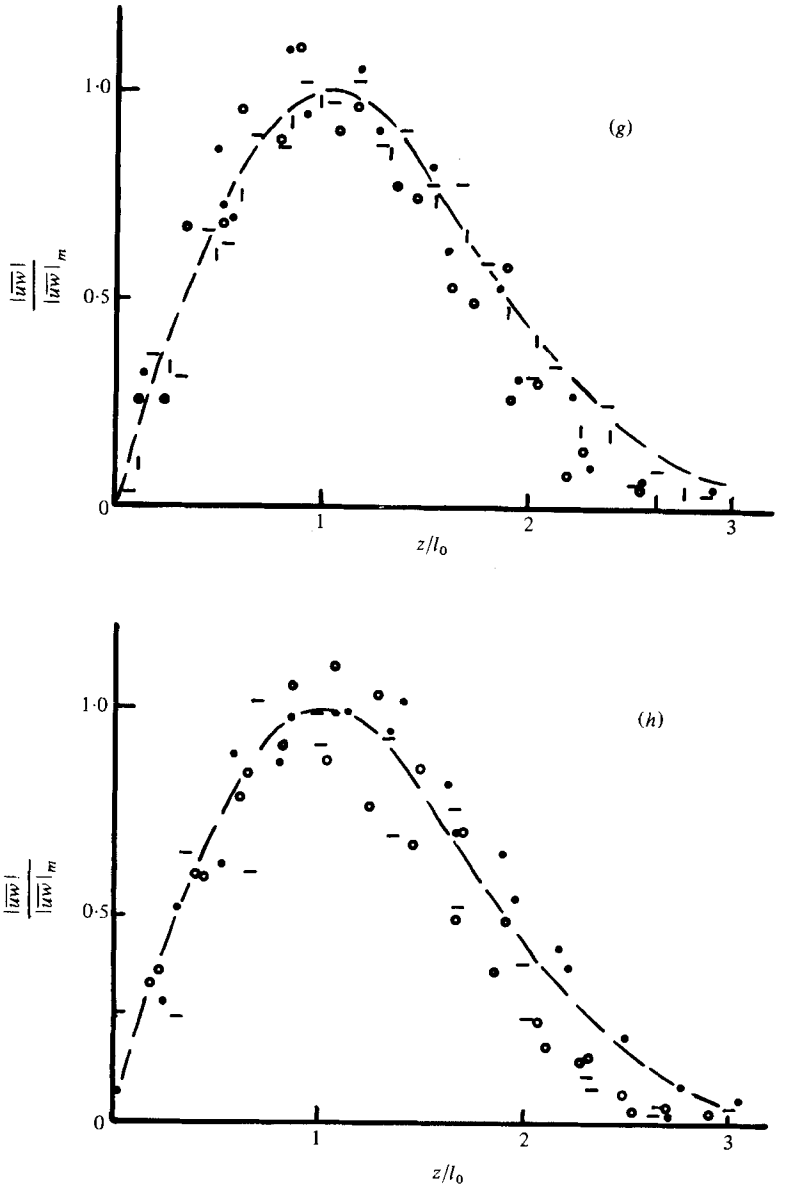

FIGURE 7. Non-dimensional distributions of turbulent intensities and Reynolds stress. (*a*, *c*, *e*, *g*) ●, x = 42 cm; ○, x = 52 cm; ——, x = 62 cm; |, x = 72 cm. (*b*, *d*, *f*, *h*) ●, x = 82 cm, ○, x = 92 cm; ——, x = 102 cm. The curves on diagrams (*g*) and (*h*) are of $e^{\frac{1}{2}}z/l_0 \exp -\frac{1}{2}(z/l_0)^2$.

6. Longitudinal gradients of velocity fluctuations

Intensities of the time-differentiated outputs from the X-wire were recorded during a series of traverses, and lateral distributions of $\overline{(\partial u/\partial x)^2}$, $\overline{(\partial w/\partial x)^2}$ and $\overline{(\partial u/\partial x)(\partial w/\partial x)}$ were calculated from them by making the 'frozen flow' approximation that $\partial/\partial t = -U\,\partial/\partial x$. The results are presented in figure 10 in non-dimensional form as ratios to the maximum values against z/l_0, and in figure 11 as the maximum values against distance from the cylinder. To remove effects of flow Reynolds number, the

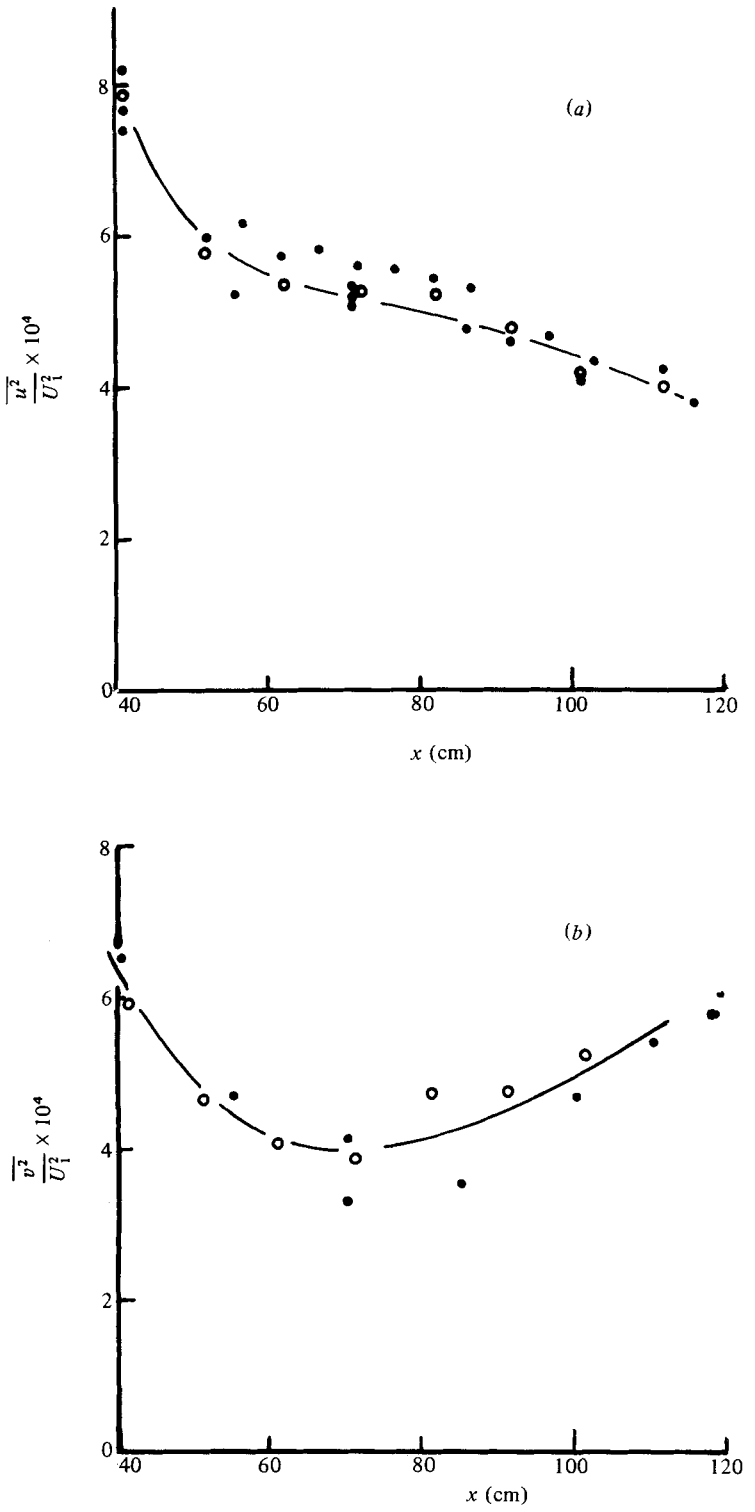

FIGURE 8 (*a*, *b*). For legend see page 449.

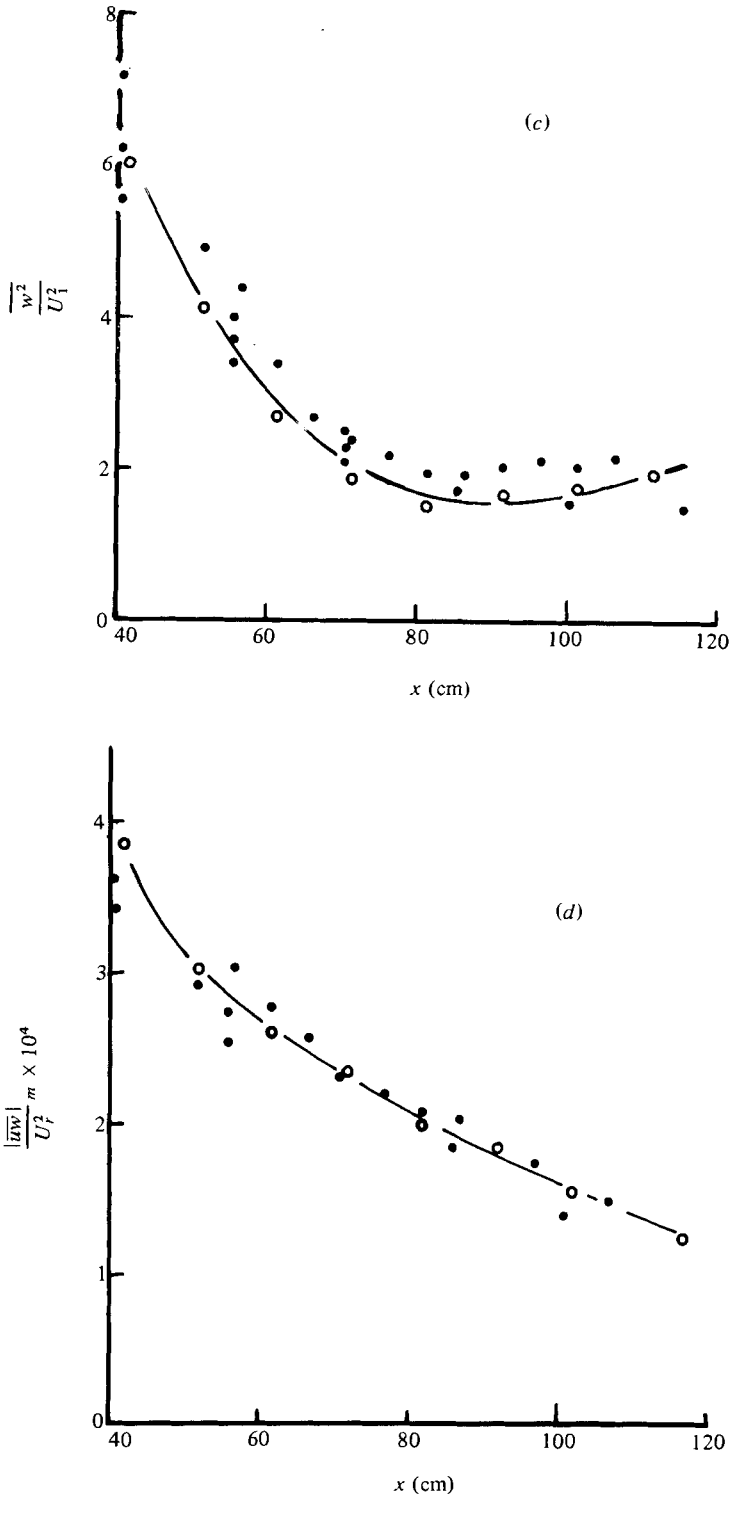

FIGURE 8. Central values of the turbulent intensities and maximum values of the Reynolds stress (from several runs).

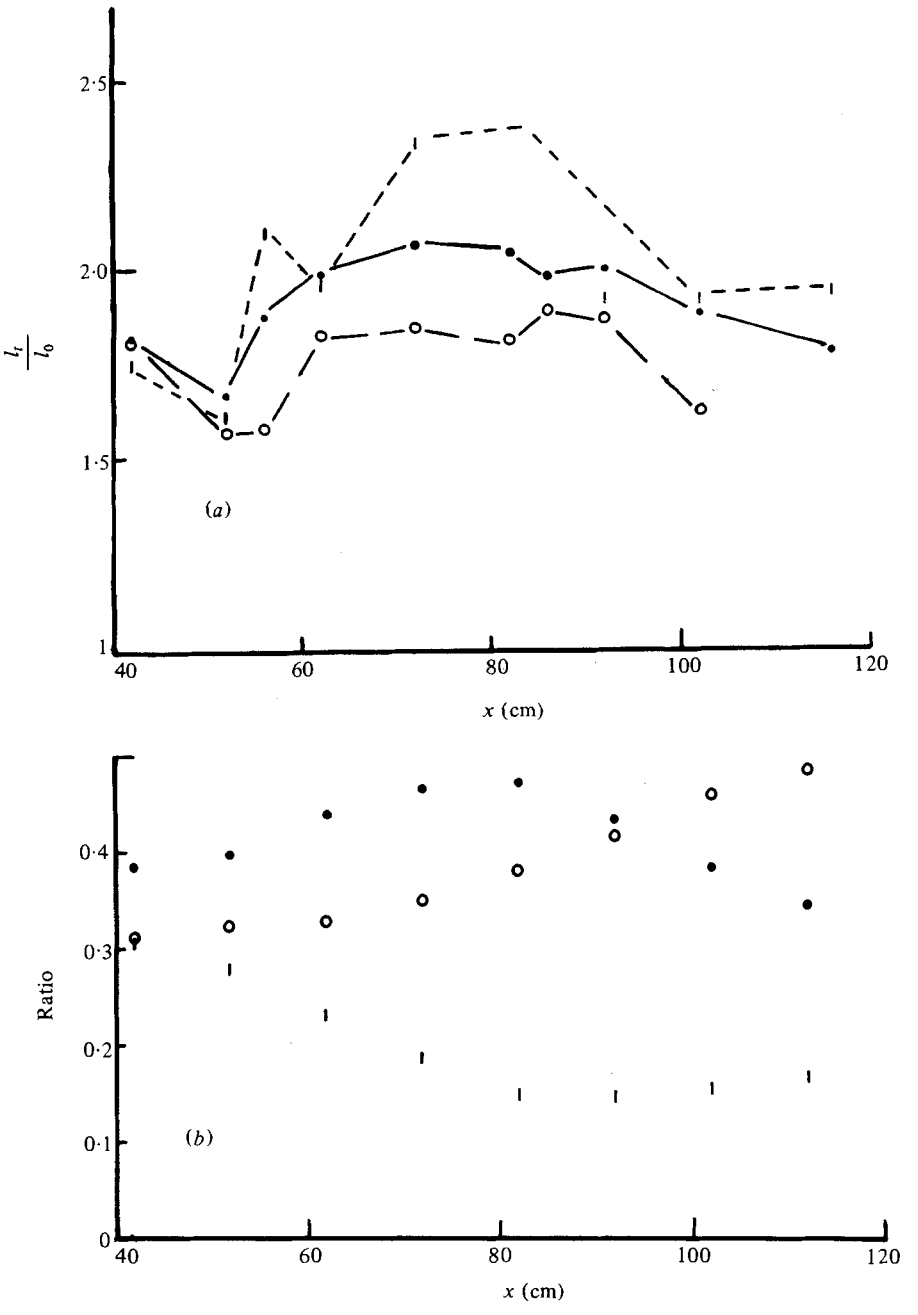

FIGURE 9. (*a*) Half-widths of the intensity distributions as fractions of the flow width: ●, from $\overline{u^2}$, ○, from $\overline{v^2}$; I, from $\overline{w^2}$. (*b*) Intensity ratios on the centre-line: ●, $\overline{u^2}/\overline{q^2}$; ○, $\overline{v^2}/\overline{q^2}$; I, $\overline{w^2}/\overline{q^2}$.

mean-square velocity gradients are given in the non-dimensional forms,

$$(\nu/U_\tau^3)\,\overline{(\partial u/\partial x)^2}, \quad \text{etc.}$$

The main features are:

(i) The distributions of $\overline{(\partial u/\partial x)^2}$ and $\overline{(\partial w/\partial x)^2}$ become more flat-topped with passage

x	$\overline{u^2}/U_r^2$	$\overline{v^2}/U_r^2$	$\overline{w^2}/U_r^2$	$\lvert\overline{uw}\rvert_r/U_r^2$	$\overline{q^2}/U_r^2$	L_u/l_0	L_v/l_0	L_w/l_0
42	$7{\cdot}5\times10^{-4}$	$6{\cdot}1\times10^{-4}$	$6{\cdot}0\times10^{-4}$	$3{\cdot}85\times10^{-4}$	$19{\cdot}6\times10^{-4}$	1·82	1·81	1·75
52	$5{\cdot}85\times10^{-4}$	$4{\cdot}75\times10^{-4}$	$4{\cdot}1\times10^{-4}$	$3{\cdot}05\times10^{-4}$	$14{\cdot}7\times10^{-4}$	1·67	1·57	1·61
62	$5{\cdot}35\times10^{-4}$	$4{\cdot}0\times10^{-4}$	$2{\cdot}8\times10^{-4}$	$2{\cdot}6\times10^{-4}$	$12{\cdot}15\times10^{-4}$	1·99	1·83	1·96
72	$5{\cdot}25\times10^{-4}$	$3{\cdot}95\times10^{-4}$	$2{\cdot}1\times10^{-4}$	$2{\cdot}35\times10^{-4}$	$11{\cdot}3\times10^{-4}$	2·07	1·85	2·34
82	$5{\cdot}2\times10^{-4}$	$4{\cdot}2\times10^{-4}$	$1{\cdot}65\times10^{-4}$	$2{\cdot}1\times10^{-4}$	$11{\cdot}3\times10^{-4}$	2·05	1·82	2·22
92	$4{\cdot}75\times10^{-4}$	$4{\cdot}55\times10^{-4}$	$1{\cdot}6\times10^{-4}$	$1{\cdot}8\times10^{-4}$	$10{\cdot}9\times10^{-4}$	2·01	1·88	1·93
102	$4{\cdot}2\times10^{-4}$	$5{\cdot}05\times10^{-4}$	$1{\cdot}7\times10^{-4}$	$1{\cdot}55\times10^{-4}$	$10{\cdot}95\times10^{-4}$	1·89	1·63	1·93
112	$4{\cdot}0\times10^{-4}$	$5{\cdot}6\times10^{-4}$	$1{\cdot}95\times10^{-4}$	$1{\cdot}25\times10^{-4}$	$11{\cdot}55\times10^{-4}$	1·79	—	1·95

TABLE 2. Turbulent intensities and scales.

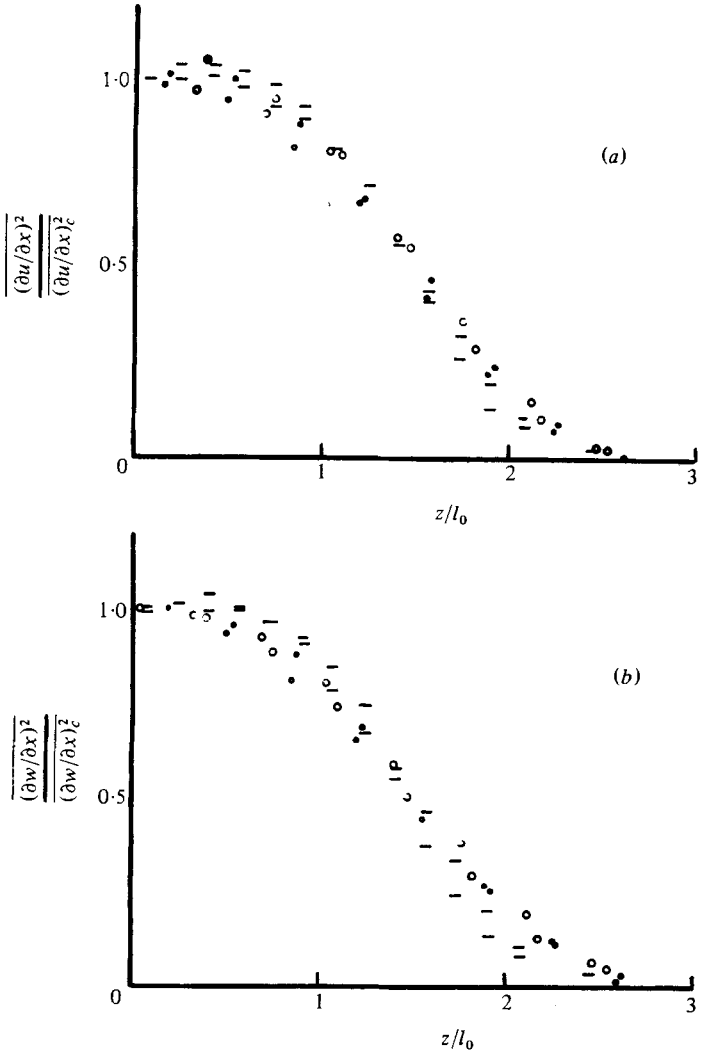

FIGURE 10. (*a*) Non-dimensional distributions of $\overline{(\partial u/\partial x)^2}$. (*b*) Non-dimensional distributions of $\overline{(\partial w/\partial x)^2}$. ●, x = 42 cm; ○, x = 72 cm; ——, x = 102 cm.

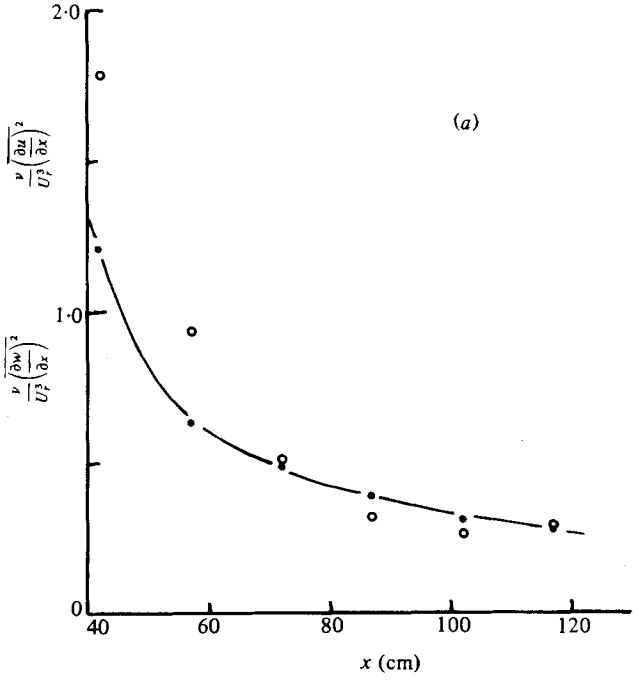

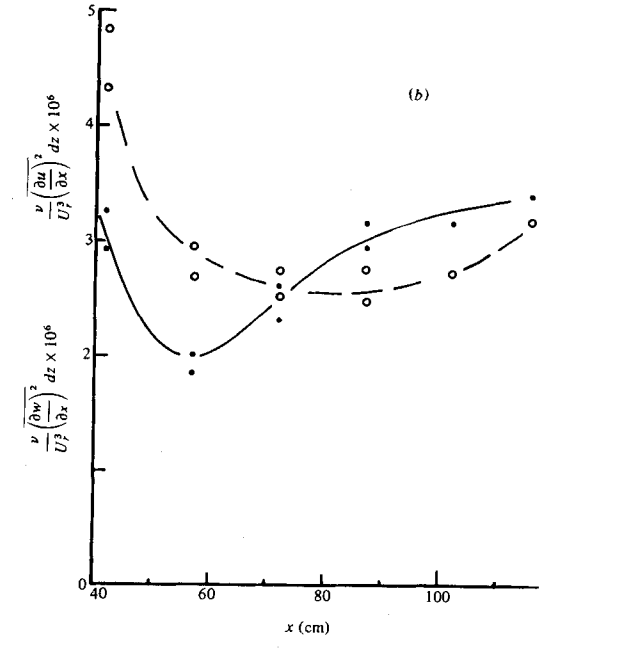

FIGURE 11. (*a*) Central values of $(\nu/U_\tau^3)\overline{(\partial u/\partial x)^2}$ (●) and of $(\nu/U_\tau^3)\overline{(\partial w/\partial x)^2}$ (○). (*b*) Values of $(\nu/U_\tau^3)\int\overline{(\partial u/\partial x)^2}\,dz$ (●) and $(\nu/U_\tau^3)\int\overline{(\partial w/\partial x)^2}\,dz$ (○).

through the distortion (compare for z/l_0 near 0·5 and near 2·0 for distances from the cylinder of 42 cm and 102 cm), perhaps because turbulent energy is being generated by the irrotational straining over the whole width of the wake.

(ii) Before entering the distortion, measured values of the ratio $\overline{(\partial u/\partial x)^2}/\overline{(\partial w/\partial x)^2}$ are near 0·7, and possibly a correction for the finite dimensions of the wire assembly would reduce it to near the 'isotropic' value of 0·5. The ratio increases through the distortion but remains less than the intensity ratio $\overline{u^2}/\overline{w^2}$.

(iii) Values of the correlation coefficient, $\overline{(\partial u/\partial x)(\partial w/\partial x)}/[\overline{(\partial u/\partial x)^2}\,\overline{(\partial w/\partial x)^2}]^{\frac{1}{2}}$, near the positions of maximum shear are about one-half of the correlation coefficient for velocity fluctuations, $|\overline{uw}|/(\overline{u^2}\overline{w^2})^{\frac{1}{2}}$.

It is apparent that the part of the turbulent motion that contributes to the velocity gradients is far from isotropic, and that the anisotropy arises both from the plane shearing of the wake and from the irrotational straining of the ambient flow. For the moderate Reynolds number of the flow, some anisotropy is not unexpected but its extent makes it necessary to treat with caution estimates of rates of turbulent energy dissipation from relations such as

$$\epsilon = 15\nu\overline{(\partial u/\partial x)^2}, \tag{6.1}$$

which assume full isotropy of the dissipating eddies.

7. Measurements of flow intermittency

The original reason for recording intermittency factors along with the turbulent intensities was to determine the location of the central plane of the wake as the average of the mean positions of the flow boundaries, but the distributions can be used to measure the rates of entrainment of non-turbulent fluid and the depths of indentation of the flow boundaries. An intermittency signal, $\delta(\mathbf{x}, t)$, intended to be zero if the flow at the position $\mathbf{x}$ is not turbulent and to be one if it is, was constructed from the outputs of the X-wire. The signal was averaged using resistance-capacity filters with time-constants of nearly five seconds, and the resulting outputs were recorded with the intensity outputs. The mean value of the intermittency signal, $\gamma(\mathbf{x}) = \overline{\delta(\mathbf{x}, t)}$, is the fraction of time that there is turbulent flow at the position of the sensor, and the recorded outputs are believed to be good approximations to it. Distributions of intermittency factor were found using both the u and w components as basic input, with no appreciable differences.

The distributions are represented very well by the difference of two error integrals,

$$\gamma(z) = (2\pi)^{-\frac{1}{2}}\left[\int_{-\infty}^{(z-z_1)/\mu} e^{-\frac{1}{2}s^2}\,ds - \int_{(z-z_2)/\mu}^{\infty} e^{-\frac{1}{2}s^2}\,ds\right], \tag{7.1}$$

where z_1, z_2 are (nearly) the positions where $\gamma = \frac{1}{2}$, and μ is the standard deviation of $\partial\gamma/\partial z$ about those positions. z_1 and z_2 define the mean positions of the bounding surfaces between fully turbulent and non-turbulent flow, and μ is a measure of the depth of the indentations of the surface. A convenient way to calculate μ is to evaluate by quadrature

$$I_\gamma = \int_{-\infty}^{\infty} (\partial\gamma/\partial z)^2\,dz. \tag{7.2}$$

x	η_0 (cm)	μ (cm)	η_0/c	u_e/U_r	μ/η_0	η_0/l_0
42	2·17	0·40	2·13		0·183	2·54
				$1{\cdot}1\times10^{-2}$		
52	2·33	0·50	2·24		0·214	2·19
				$0{\cdot}9\times10^{-2}$		
62	2·92	0·66	2·32		0·228	2·40
				$0{\cdot}1\times10^{-2}$		
72	3·56	0·84	2·33		0·235	2·15
				$2{\cdot}8\times10^{-2}$		
82	4·81	1·19	2·49		0·233	2·22
				$7{\cdot}7\times10^{-2}$		
92	6·64	1·39	2·85		0·209	2·34
				$4{\cdot}4\times10^{-2}$		
102	8·00	1·42	3·03		0·178	2·24
				$12{\cdot}8\times10^{-2}$		
112	8·3	1·78	3·50		0·214	1·97

TABLE 3. Results from intermittency values.

If the distribution is of the form (7.1) and if $\mu^2 \ll (z_1-z_2)^2$,

$$\mu = (\pi^{\frac{1}{2}} I_\gamma)^{-1}. \tag{7.3}$$

The values of $\eta_0 = \frac{1}{2}(z_1-z_2)$ and μ given in table 3 are sufficient to describe completely the recorded distributions.

In principle, the rate of entrainment of non-turbulent fluid into the wake can be calculated from the measured values of η_0, b and c, using the relation

$$u_e/U_r = b^{-1} d(\eta_0/c)/dx, \tag{7.4}$$

equivalent to equation (3.13). Unfortunately, η_0 and the lateral strain ratio c increase together and, particularly towards the end of the distortion, gradients of η_0/c determined by finite difference are very sensitive to the values of the strain ratio. The values of the non-dimensional entrainment velocity, u_e/U_r, listed in table 3 have been obtained by drawing a smooth curve through values of η_0/c plotted against x (figure 12*a*) and using values of b and c from table 1.

The measured values of the entrainment velocity decrease from $1{\cdot}1\times10^{-2}U_r$ at $x = 47$ cm (with a probable error estimated at 25 %) to $0{\cdot}1\times10^{-2}U_r$ at $x = 67$ cm, increasing to $2{\cdot}8\times10^{-2}U_r$ at $x = 77$ cm. In a plane wake, the entrainment ratio, u_e/u_0, is 0·21 for comparable distances from the cylinder (Townsend 1976, table 6.5), while the measured ratios for $x = 47, 67, 77$ cm are 0·16, 0·02 and 0·4 respectively. The decrease in entrainment is expected from the effect of lateral compression on the entrainment eddies, and, although the numerical uncertainty is considerable, the recovery of entrainment velocity near $x = 77$ cm is thought to be real. From that point, the calculated values are too large to be believed. They exceed considerably the root mean square of the total velocity fluctuation, $3{\cdot}3\times10^{-2}U_r$ (see table 2), and it is likely that the wake is spreading by secondary flows generated as the wake width becomes comparable with the channel depth.

Only small changes are found in the relative depth of the boundary indentations, μ/η_0, and in the ratio of the mean width of the turbulent flow to the mean velocity length scale, η_0/l_0 (figure 12*b*). The width ratio remains nearly constant with an

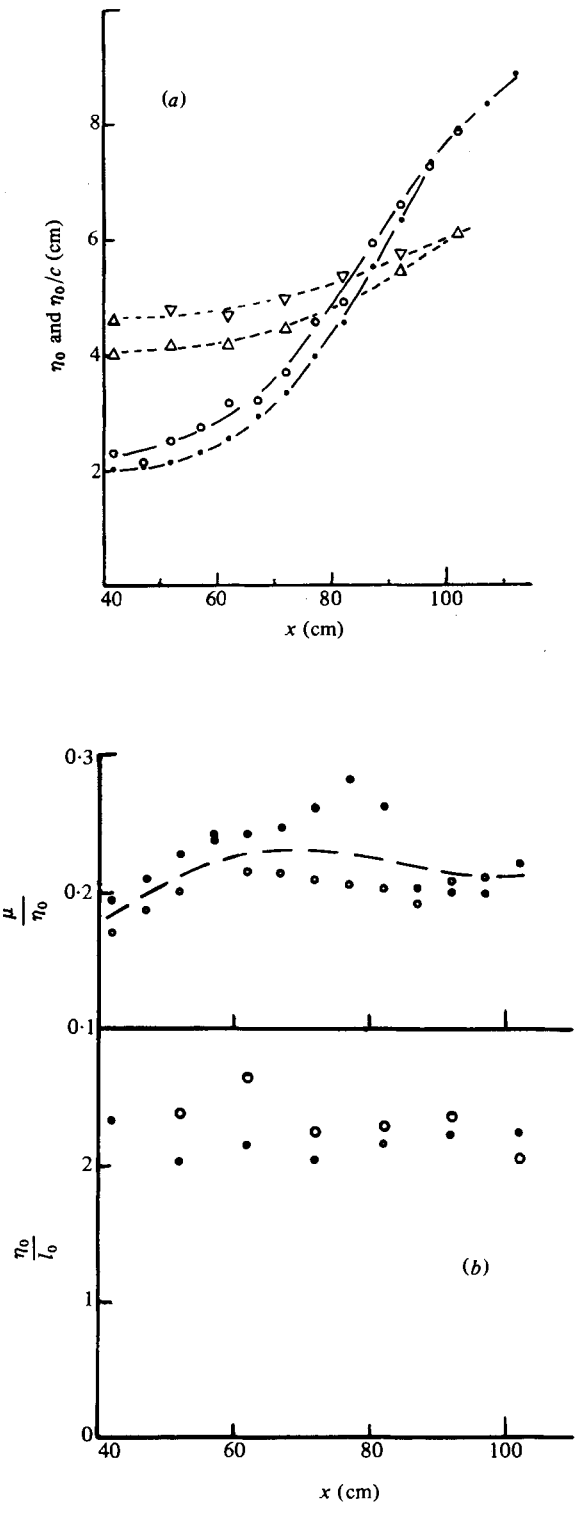

FIGURE 12. Parameters of the intermittency distributions. (*a*) Values of η_0 (●, ○) and of η_0/c (△, ▽). (*b*) Values of η_0/l_0 and of μ/η_0.

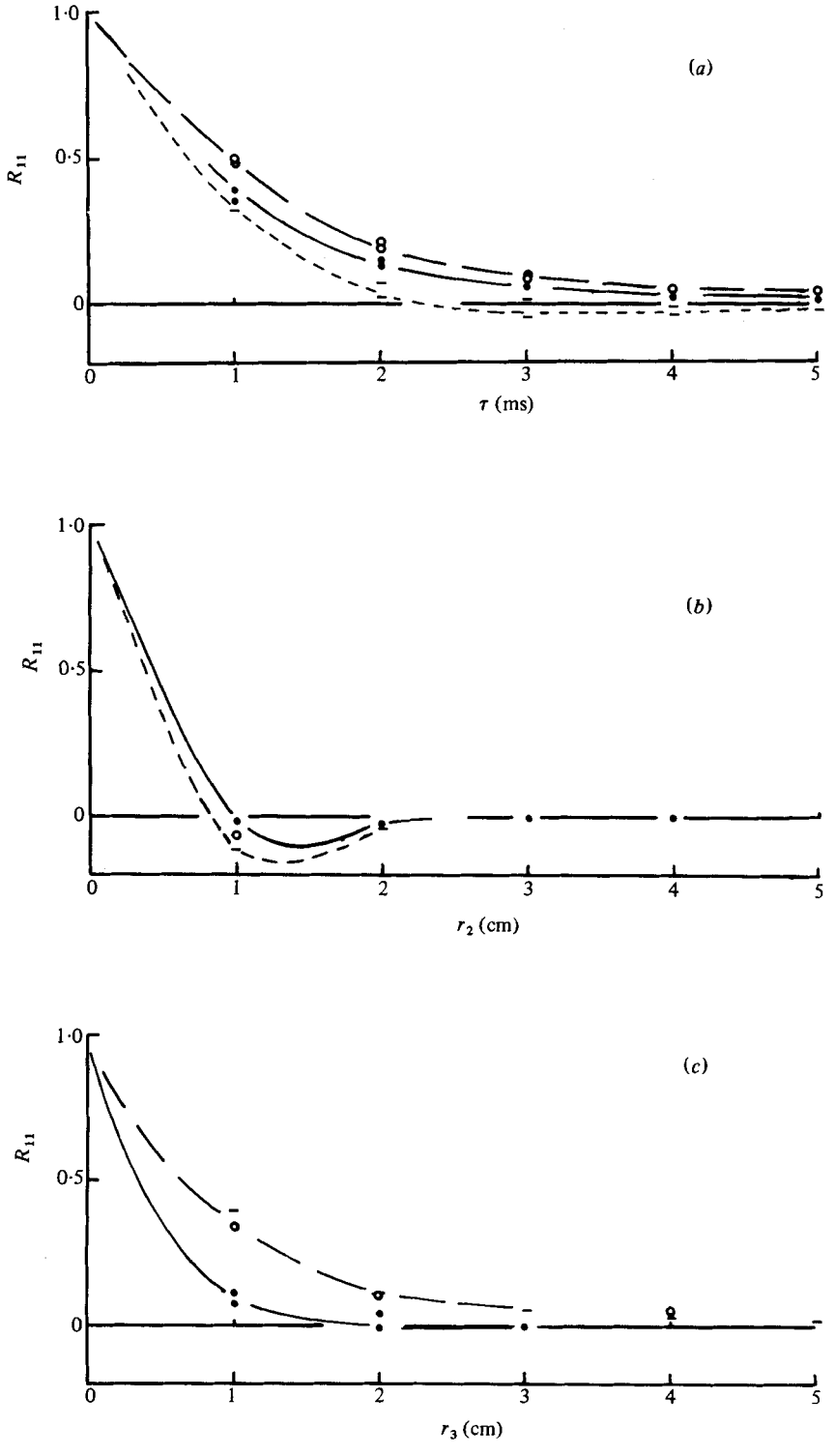

FIGURE 13. One-dimensional correlations $R_{11}/\overline{u_1^2}$. (*a*) Autocorrelation $R_{11}(0, \tau)$, (*b*) Oy correlations $R_{11}(0, r, 0)$, (*c*) Oz correlation $R_{11}(0, 0, r)$. ●, x = 42 cm; ○, x = 72 cm; ——, x = 102 cm.

average value of 2·2, to be compared with values of 2·1 in plane wakes and jets (Townsend 1976, table 6·2). The relative depth varies from 0·23 near $x = 70$ cm to 0·20 near the entrance and exit from the distortion.

8. Velocity correlations and longitudinal spectra

By recording the velocity fluctuations from arrays of eight hot wires set in a line across the flow, space–time correlations such as

$$R_{11}(\mathbf{r}, \tau; z) = \overline{u_1(\mathbf{x}, t)\, u_1(\mathbf{x}+\mathbf{r}, t+\tau)} \tag{8.1}$$

can be calculated for sensor separations $\mathbf{r}$ set by the array geometry and time differences τ that are multiples of the sampling interval. Figure 13 shows the auto-correlation $R_{11}(0, \tau; z)$, and the two spatial correlations, $R_{11}(0, r, 0; z)$ and $R_{11}(0, 0, r; z)$, for the reference wire near the central plane of the wake and at three distances from the cylinder, expressed as fractions of the turbulent intensity at the reference wire.

Between $x = 41$ cm, before entering the distortion, and $x = 71$ cm, the time scale of the auto-correlation increases by about 30 %, but thereafter the scale appears to decrease sharply. The apparent decrease is a consequence of the change from a correlation monotonically decreasing with time delay to one with negative values over a range of time delays similar to those for appreciable correlation before. A similar change would be expected in grid turbulence as it is known that the spectrum develops a maximum for lateral strain ratios in excess of 2 (Townsend 1954).

The transverse correlations for separations parallel to the cylinder axis and so in the direction of lateral compression, $R_{11}(0, r, 0)$, show a steady but small decrease in scale, far less in ratio than the total strain b. Between $x = 41$ cm and $x = 71$ cm, the other transverse correlation, $R_{11}(0, 0, r)$, increases in scale roughly in proportion to the total strain ratio c, but no further increase occurs in spite of further extension.

Frequency spectra of velocity fluctuations in the xOz plane have been calculated from digital records of the outputs from X-wires, with a sampling interval of 0·256 ms. They have been rescaled to give one-dimensional spatial spectra on the assumption that the 'frozen flow' approximation is valid. Figure 14 shows the spectra for $x = 41$ cm and for $x = 85$ cm as plots of $k\phi_{ij}(k)$ against a logarithmic scale of the longitudinal wavenumber k. For each set, the X-wire was placed near the position of maximum shear. Spectral intensities are scaled so that

$$\int_0^\infty \phi_{ij}(k)\, dk = \overline{u_i u_j} \tag{8.2}$$

and the mode of plotting is such that areas under the spectral curves correspond with the contributions to $\overline{u_i u_j}$ from wavenumbers in the particular range.

The main features of the spectra are:

(i) Even for the largest wavenumbers, ratios of the spectral intensities are far from those expected if the motion were isotropic, i.e.

$$\phi_{33} = \tfrac{1}{2}(\phi_{11} - k\, d\phi_{11}/dk). \tag{8.3}$$

(ii) The spectral intensity of the Reynolds shear stress, $-\phi_{13}$, becomes small compared with both ϕ_{11} and ϕ_{33} for wavenumbers over 8 cm^{-1}.

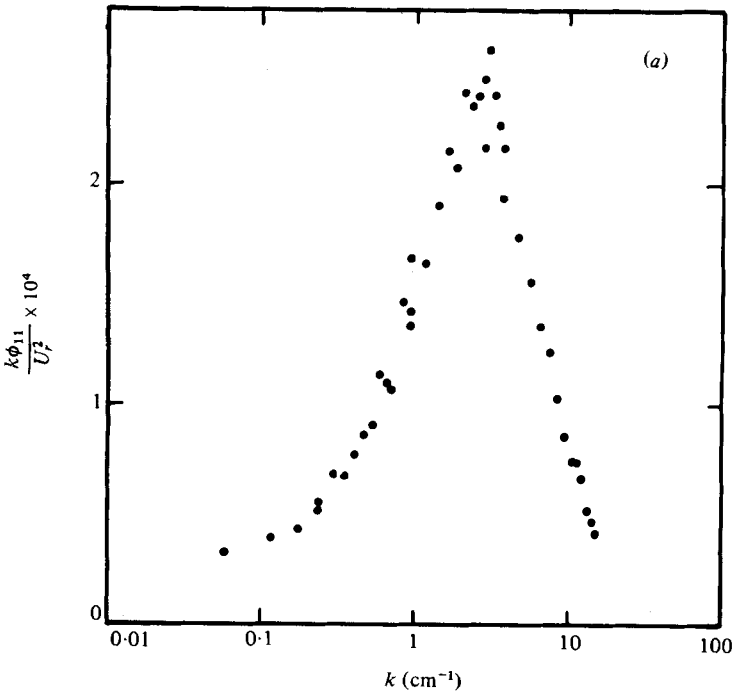

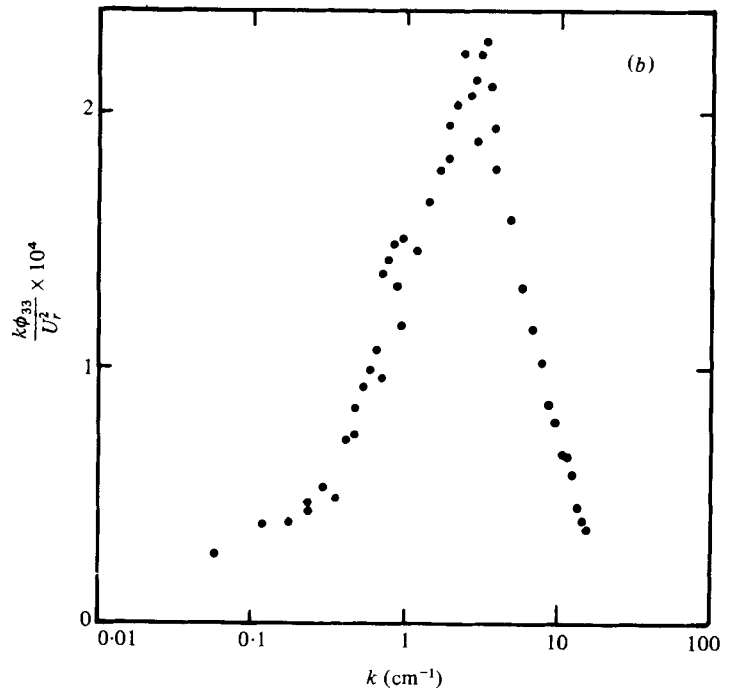

FIGURE 14(*a*, *b*). For legend see page 460.

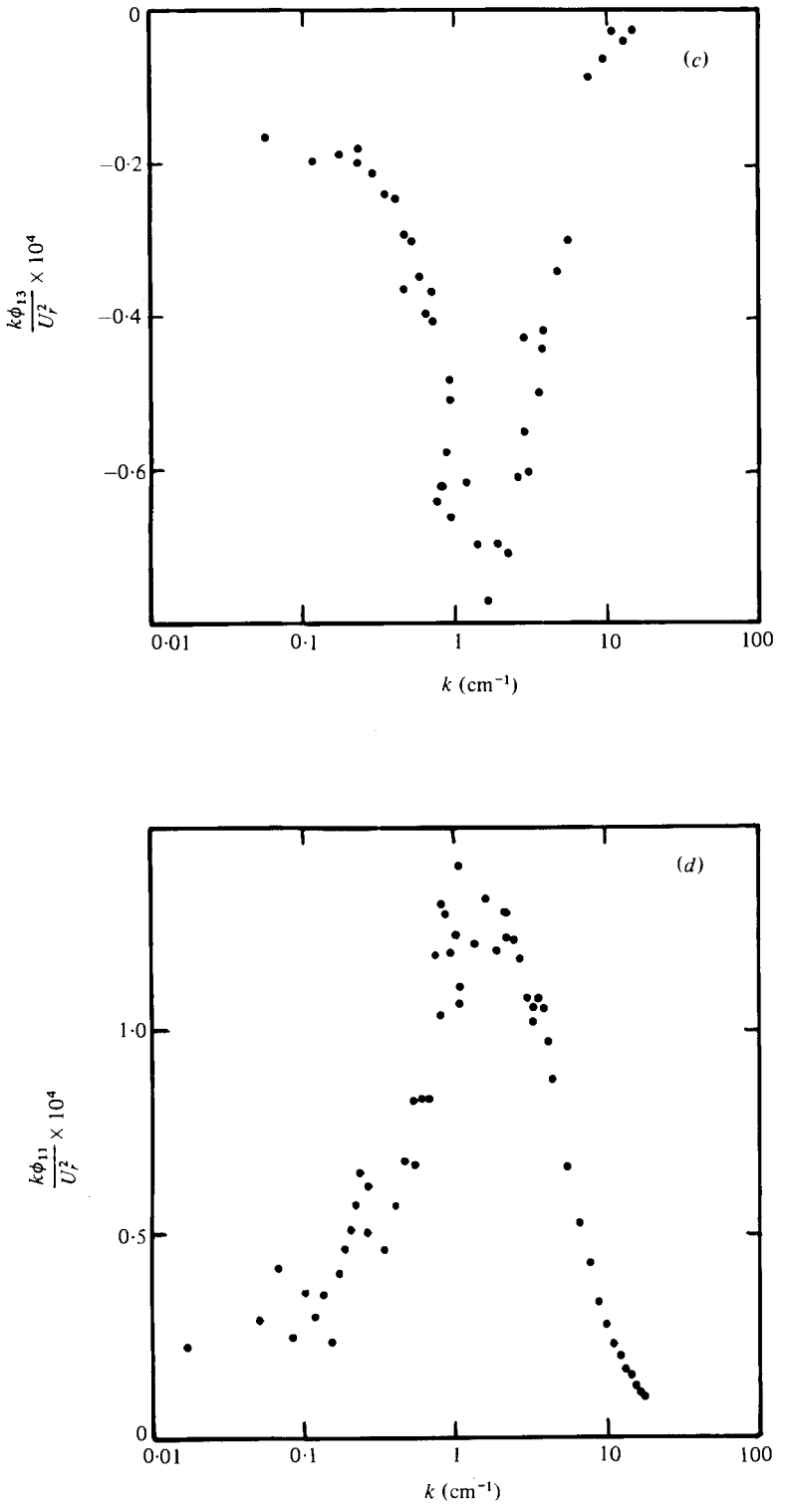

FIGURE 14 (*c*, *d*). For legend see page 460.

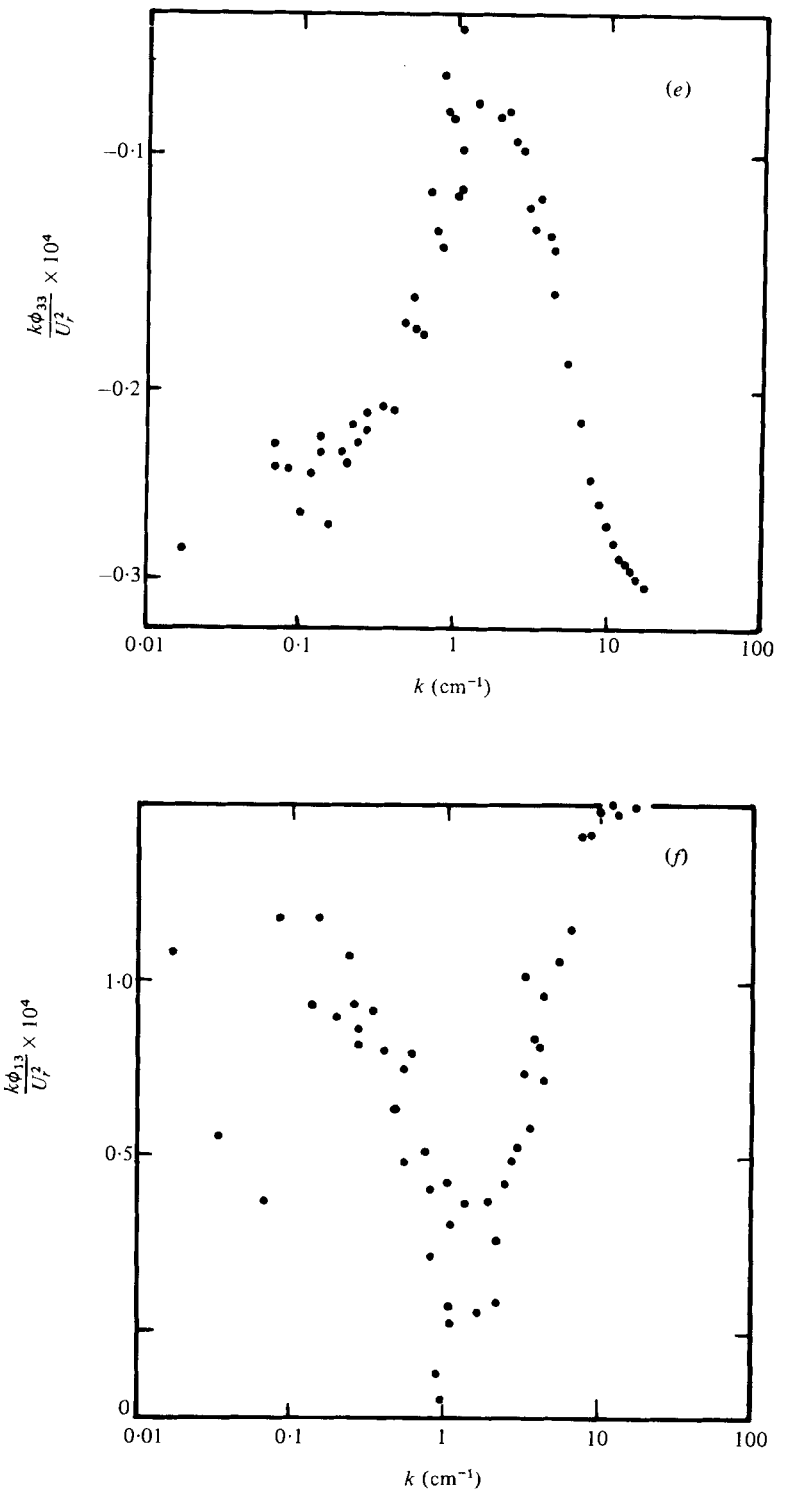

FIGURE 14. Spectra of the Ox and Oz velocity components: (a, b, c) for $x = 42$ cm, (d, e, f) for $x = 85$ cm.

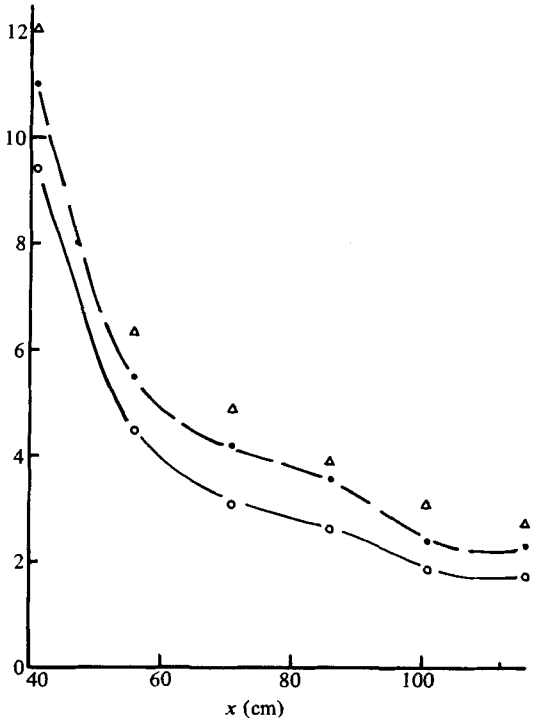

FIGURE 15. Maximum values of $k^{\frac{5}{2}}\phi^{\frac{3}{2}}U_r^{-3}$ compared with values of $10\nu\overline{(\partial u/\partial x)^2}\,U_r^{\pm 3}$ on the centre-line. ●, $(\phi_{11}^{\frac{3}{2}}k^{\frac{5}{2}}/U_r^3)\times 10^6$; ○, $(\phi_{33}^{\frac{3}{2}}k^{\frac{5}{2}}/U_r^3)\times 10^6$; △, $(10\nu\overline{(\partial u/\partial x)^2}/U_r^3)\times 10^6$.

(iii) The maximum values of $k\phi_{11}$ and $k\phi_{33}$ occur at wavenumbers decreasing from $2{\cdot}4\,\mathrm{cm}^{-1}$ at $x = 41$ cm to $1{\cdot}6\,\mathrm{cm}^{-1}$ at $x = 101$ cm.

If the small-scale motion were locally isotropic, a substantial part of the spectra would be described by

$$\phi_{11} = C\epsilon^{\frac{2}{3}}k^{-\frac{5}{3}} \tag{8.4}$$

and it would be possible to calculate the rate of turbulent energy dissipation (from a variety of sources, C is near 0·5). Unfortunately, the Reynolds number of the wake is too low for a substantial range of variation as $k^{-\frac{5}{3}}$, but, from measurements in turbulent jets, Bradshaw (1967) has found that, on a log–log plot, the line representing equation (8.4) with an energy dissipation found from the energy balance is nearly tangential to the measured spectrum. The energy dissipation is an important quantity but difficult to measure in the distorted wake, and Bradshaw's observation suggests that the maximum values of $k^{\frac{5}{2}}\phi^{\frac{3}{2}}$ may be a fair approximation to $C^{\frac{3}{2}}\epsilon$. In figure 15, maximum values of $U_r^{-3}k^{\frac{5}{2}}\phi_{11}^{\frac{3}{2}}$ and $U_r^{-3}k^{\frac{5}{2}}\phi_{33}^{\frac{3}{2}}$ are plotted against distance from the cylinder and compared with central values of $10U_r^{-3}\overline{(\partial u/\partial x)^2}$. The similarity of the variations with downstream distance suggests that, while the absolute values are uncertain, the relative variation is reliable.

9. Production and dissipation of turbulent energy

The relative effects of the shearing and the irrotational distortion on the turbulent motion may be measured by the respective mean valocity gradients or by the rates of

energy transfer to the motion. From the data in Table 1, the maximum rate of shear changes from about $40\,s^{-1}$ at $x = 42$ cm to $8\,s^{-1}$ at $x = 102$ cm, to be compared with lateral rates of strain of up to $23\,s^{-1}$ and longitudinal rates of strain up to $10\,s^{-1}$. Corresponding changes take place in rates of energy transfer from the various components of the velocity gradient.

The energy balance of the whole flow is expressed by the equation for the total turbulent kinetic energy,

$$b^{-1}U_r\frac{d}{dx}\left[\frac{1}{c}\int \tfrac{1}{2}\overline{q^2}\,dz\right]+\int[\overline{u^2}-\tfrac{1}{2}(\overline{v^2}+\overline{w^2})]\,(\partial U_1/\partial x)\,dz$$

$$+\int \tfrac{1}{2}(\overline{u^2}-\overline{v^2})\,(\partial V_1/\partial y-\partial W_1/\partial z)\,dz+\int \overline{uw}\,\partial U/\partial z+\int \epsilon\,dz=0. \qquad (9.1)$$

The equation is obtained from equations (3.8) and (3.9). The several terms have been calculated from the observed mean velocities and intensities except for the total energy dissipation which has been obtained by difference. It may be pointed out that the term omitted in the derivation of equation (3.8), $d/dx\int \frac{1}{2}\overline{q^2}(U-U_1)\,dz$, is less in magnitude than $5\times10^{-6}U_r^3$ at all positions. The term representing the total energy production by shear, $\int \overline{uw}(\partial U/\partial z)\,dz$, has been calculated by assuming error law profiles for (U_1-U) and for $\overline{uw}$ so that

$$\int -\overline{uw}\,(\partial U/\partial z)\,dz = \tfrac{1}{2}(\pi e)^{\frac{1}{2}}\,u_0\,|\overline{uw}|_m. \qquad (9.2)$$

The several terms of equation (9.1) are listed in table 4. Possible errors in the calculated values of the total dissipation are large, particularly towards the end of the distortion where the magnitude of the first (advection) term is sensitive to the exact values chosen for the strain ratios and where the width of the wake has become an appreciable fraction of the channel height.

A useful index of turbulent energy dissipation is the dissipation length scale, defined as

$$L_\epsilon = (\overline{q^2})^{\frac{3}{2}}/\epsilon, \qquad (9.3)$$

which, in ordinary, almost two-dimensional flows, is in proportion to the flow width. Average values for the distorted wake have been calculated from the total dissipation, the total turbulent intensity and the width scale η_0 by the relation

$$L_\epsilon = \left[\int \overline{q^2}\,dz\right]^{\frac{3}{2}}(2\eta_0)^{-\frac{1}{2}}\Big/\int \epsilon\,dz. \qquad (9.4)$$

In effect, it assumes that intensity and local dissipation rate are distributed uniformly over a region of width $2\eta_0$. In table 5, values of L_ϵ and of L_ϵ/l_0 are given and compared with values calculated from the measurements of spectra and intensities of velocity derivatives, on the assumptions leading to equations (6.1) and (8.4) for the local rate of energy dissipation.

Estimates of L_ϵ from values of $\overline{(\partial u/\partial x)^2}$ are consistently larger than those from the spectra in a ratio close to 1·5, while the estimates from the energy balance are scattered

x	Advection	Lateral	Longitudinal	Dissipation	Shear
47	-76×10^{-6}	-1×10^{-6}	3×10^{-6}	102×10^{-6}	-33×10^{-6}
57	0	-5×10^{-6}	-11×10^{-6}	40×10^{-6}	-24×10^{-6}
67	16×10^{-6}	-13×10^{-6}	-17×10^{-6}	36×10^{-6}	-22×10^{-6}
77	30×10^{-6}	-36×10^{-6}	-5×10^{-6}	30×10^{-6}	-20×10^{-6}
87	-13×10^{-6}	-58×10^{-6}	20×10^{-6}	68×10^{-6}	-17×10^{-6}
97	-42×10^{-6}	-67×10^{-6}	28×10^{-6}	94×10^{-6}	-13×10^{-6}
107	24×10^{-6}	-30×10^{-6}	0	17×10^{-6}	-10×10^{-6}

Note: The terms are:

Advection $b^{-1}U_r^{-2}d/dx[\int c^{-1}\frac{1}{2}\overline{q^2}dz]$

Lateral production $\frac{1}{2}(\partial V_1/\partial y-\partial W_1/\partial z)\,(\overline{v^2}-\overline{w^2})\,U_r^{-3}$

Longitudinal production $(\partial U_1/\partial x)\,(\overline{u^2}-\frac{1}{2}(\overline{v^2}+\overline{w^2}))\,U_r^{-3}$

Dissipation (by difference) $U_r^{-3}\int\epsilon dz$

Shear production $U_r^{-3}\int\overline{uw}(\partial U/\partial z)\,dz$

Negative values represent a net gain, positive ones a net loss.

TABLE 4. Terms in the energy balance equation.

	L_ϵ (cm)			L_ϵ/l_0		
x	Balance	$(\overline{\partial u/\partial x})^2$	Spectra	Balance	$(\overline{\partial u/\partial x})^2$	Spectra
42	—	4·78	2·79	—	5·6	3·3
47	2·19	—	—	2·3	—	—
52	—	5·16	3·16	—	4·5	2·8
57	3·86	—	—	3·4	—	—
62	—	—	—	—	—	—
67	4·74	—	—	3·3	—	—
72	—	5·22	3·20	—	3·1	1·9
77	7·42	—	—	3·9	—	—
82	—	—	—	—	—	—
87	4·48	6·30	3·62	1·8	2·5	14
92	—	—	—	—	—	—
97	3·65	—	—	1·1	—	—
102	—	7·92	5·34	—	2·2	1·5
107	20·7	—	—	5·4	—	—
112	—	9·52	6·03	—	2·3	1·4

TABLE 5. Dissipation length scales.

but tend to lie between them. An exception is the value for $x = 47$ cm, where the advection term in the energy balance is large and may be overestimated by up to 30 % by finite-difference calculation of the longitudinal derivative in equation (9.1). Along the distortion, the dissipation length scale increases by a factor of around two while the flow width increases by a factor of four. Correspondingly, the ratio L_ϵ/l_0 decreases from nearly three, characteristic of wakes and jets developing in uniform flow, to about 1·5 at the end of the distortion.

Energy production from shear decreases through the distortion and becomes much less than the rate of production from the irrotational distortion. Although the production from longitudinal stretching changes sign in the second half of the distortion, the total of longitudinal and lateral production becomes nearly constant.

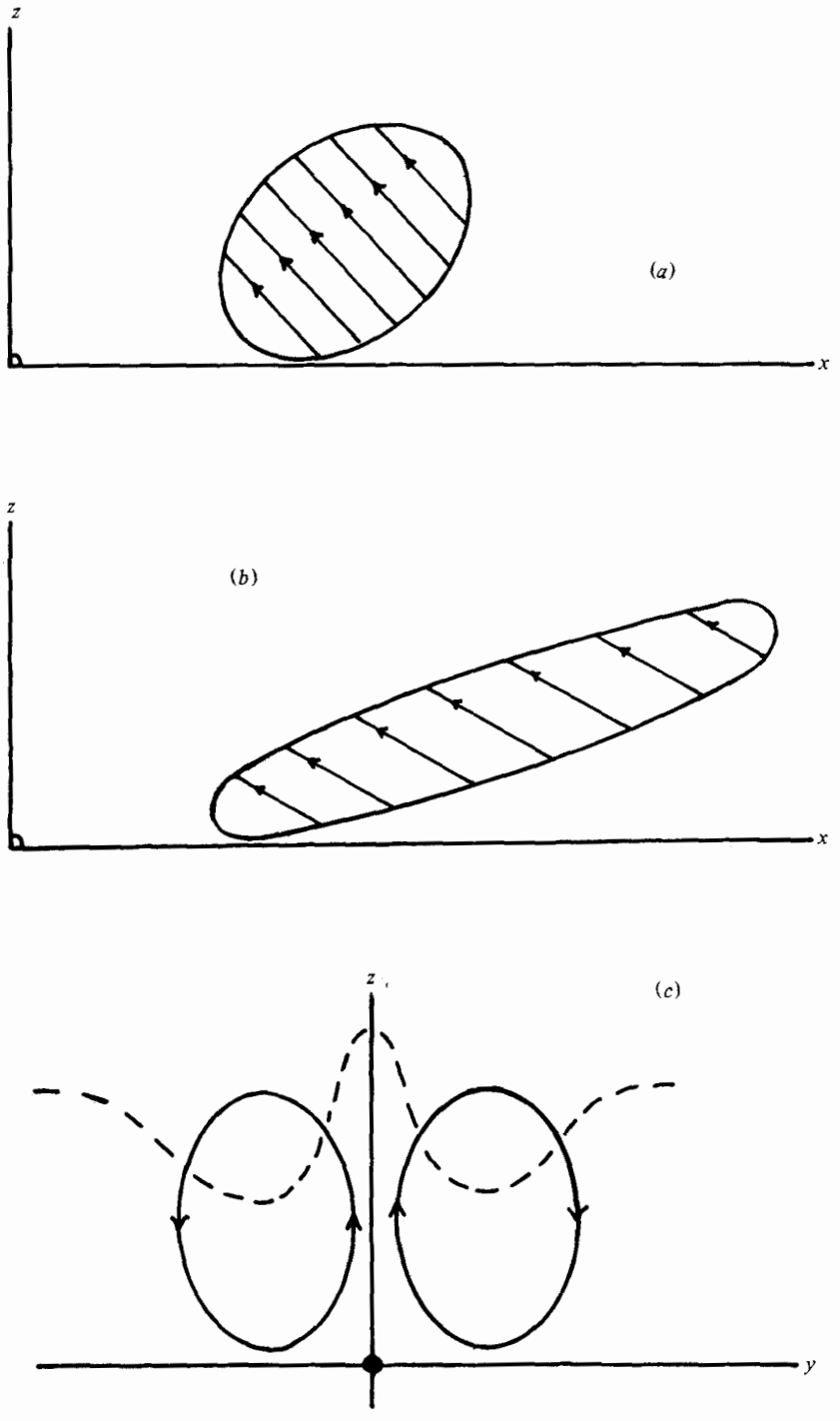

FIGURE 16. Development of long roller eddies in the distorted wake. (*a*) Section of a typical hairpin eddy in an undistorted wake. Active entrainment disrupts the eddies before they can be elongated any more. (*b*) Section of an hairpin eddy that has been elongated by the shearing in the absence of active entrainment. (*c*) Transverse section of an elongated eddy, showing the folding of the bounding surface. (The arrows indicate the planes of circulation, or, in (*c*), streamlines.)

10. Discussion

The distorted wake differs in two significant respects from most of the turbulent flows which have been studied in detail. First, the turbulent motion receives energy both from the velocity shear of the wake and from the externally generated irrotational flow. Second, the external distortion extends eddies in the direction of shear while compressing them in the spanwise direction. If the flow patterns were distorted in proportion to the strain ratios, eddies with aspect ratios around 9 : 1 would emerge from the distortion.

An effect of the distortion is to change the ratios of the turbulent intensities in nearly the way that has been observed in grid turbulence passing through similar distorting ducts (Maréchal 1967; Tucker & Reynolds 1968), and that would be expected either from consideration of transport equations or from forms of rapid-distortion theory (Townsend 1980). The initial increase in the ratio of Reynolds shear stress to total intensity is common to all the runs, and it seems to be consequent on the initial flow acceleration between $x = 42$ cm and $x = 52$ cm. From there on, the ratio decreases steadily as would be expected if the irrotational straining transfers energy to the motion without generating Reynolds stress.

In plane wakes, entrainment of ambient fluid is carried out by groups of large eddies with circulations in the xOz plane, which distort the bounding surface and so continuously increase the area over which entrainment can occur (Grant 1958; Keffer 1965). In Keffer's experiments on the distorted wake, the direction of stretching was parallel to the cylinder axis and energy is transferred to these eddies, leading to a large increase in the rate of entrainment. With the direction of compression parallel to the axis, the entrainment eddies lose energy, cease to distort further the bounding surface and the entrainment rate falls sharply (table 3). Near the middle of the distortion, the rate has recovered to near the original value, indicating that the bounding surface is being distorted by large eddies whose motion is not inhibited by the axial compression. Records of intermittency factor suggest that the new entrainment eddies may be long roller eddies with axes in the flow direction and little vorticity in the direction of shear. It is possible that the new eddies could arise as double-roller or hairpin eddies, developed in response to the shearing and able, in the absence of disruption by the original entrainment eddies, to endure until they become inclined at small angles to the mean flow by the action of the shearing. Figure 16 attempts to illustrate the process. In an unstrained wake, the energy- and stress-containing eddies become elongated by the shear only to the extent indicated in figure 16(*a*) before being broken up by active entrainment. If the entrainment eddies are removed by lateral distortion, elongation may continue until energy-containing eddies have forms resembling that in figure 16(*b*). The consequence for the bounding surface is indicated in figure 16(*c*), which shows a transverse section of the flow and a double-roller eddy.

The relative depth of the indentations of the bounding surface, measured by μ/η_0 (figure 12 and table 3), changes much less than the entrainment rates, in apparent conflict with the correlation found by Gartshore (1966). However, removal of energy from the original entrainment eddies may prevent further growth of the indentations but they can be filled in only by slow, small-scale local entrainment. Similarly, new entrainment eddies must indent the surface to a considerable extent before the rate of increase of surface area is sufficient to cause an increase in entrainment. In short, while

entrainment is small, the indentations produced by the original eddies are slowly filling and the new eddies are indenting the surface but not yet at a rate to produce effective entrainment. The correlation between relative depth and entrainment found by Gartshore for self-preserving flows requires similarity of the entrainment mechanism at all stages of flow development, and will not be valid in flows like the distorted wake.

The change in shape of the distributions of $\overline{w^2}$, the intensity of fluctuations normal to the plane of the wake (figures 7*e*,*f*), is probably a consequence of the suppression of the original entrainment eddies. In a plane wake, these eddies have motions in the xOz plane roughly described by stream functions of the form

$$\psi(x,z) = A\,\mathrm{sech}\,(kz)\cos(kx), \tag{10.1}$$

where, near any particular section, the wavenumber k varies over a range of about 1·3 : 1 (Townsend 1979). The consequent contributions to the intensities are

$$\left.\begin{aligned}(\overline{u^2})_e &= \tfrac{1}{2}A^2k^2\tanh^2(kz)\,\mathrm{sech}^2(kz)\\ \text{and}\qquad (\overline{w^2})_e &= \tfrac{1}{2}A^2k^2\,\mathrm{sech}^2(kz),\end{aligned}\right\} \tag{10.2}$$

and the contribution to $\overline{w^2}$ is a maximum at the wake centre while the contribution to $\overline{u^2}$ is small at the centre with maxima near the positions of maximum shear. Suppression of eddies of this form would reduce values of $\overline{w^2}$ at the wake centre more than near positions of maximum shear and might easily lead to the appearance of the central minimum.

Distortion by the irrotational straining has a considerable effect on the length scales of the turbulent motion. The correlations show little change of eddy extent in the direction of compression in spite of an overall strain ratio of nearly three, possibly because the large energy-containing eddies are expanding in that direction by turbulent diffusion at nearly the same rate as they are being compressed by the mean flow gradient (figure 13*b*). In the downstream direction, the extent appears to decrease sharply beyond $x = 80$ cm, but the decrease is almost entirely in the extent of positive correlation and the negative correlations for delays over 2 ms (figure 13*a*) extend for nearly as far as the original positive ones. In the direction of lateral extension, a considerable increase of scale occurs between $x = 42$ cm and $x = 72$ cm, but little to no change with further extension (figure 13*c*). A natural interpretation is that an eddy becomes unstable if it is too elongated, and that it breaks up into sections of smaller aspect ratio, each having a motion nearly similar to that which it had before the break. It appears that the scales in the two transverse directions are roughly equal on entry to the distorting duct, but, after a distortion ratio of 2·5 : 1 (ratio of extension in Oz direction to that in the Oy direction), the ratio of scales attains a limiting value near 2 : 1.

The changes of the correlation scale in the spanwise Oz direction are similar in ratio to those in the dissipation length scale (table 4), and the ratios to the flow width each decrease by a factor of two. In simple flows, all the length scales of the turbulent motion are proportional to and presumably controlled by the width of the mean velocity distribution, but prolonged lateral distortion with extension in the direction of shear leads to scales much less than the mean velocity scale and, apparently, to scales not controlled by it.

To summarize the main conclusions from the measurements:

(i) The distributions of velocity defect, turbulent intensities, Reynolds shear stress

and intermittency change very little in shape during the passage of the wake through the distortion, the ratios of the several widths remain nearly constant.

(ii) The initial effect of the lateral distortion is to reduce considerably the rate of entrainment, but, after a total strain of 2 :1, the rate recovers to near the original value. The renewed entrainment is thought to arise from the generation of entrainment eddies that do not lose energy to the distorting velocity field.

(iii) Length scales of the turbulent motion increase through the distortion but by much less than the flow width. On emergence, the scales have become small compared with the flow width.

(iv) The ratio of Reynolds stress to total intensity increases during initial flow acceleration but decreases steadily with increasing lateral distortion.

Support for the work came from the Science Research Council and from the Berkeley Nuclear Laboratory of the Central Electricity Generating Board.

REFERENCES

BRADSHAW, P. 1967 *National Physical Laboratory, Aero. Rep.* no. 1220.
ELLIOTT, C. J. 1976 Ph.D. dissertation, University of Cambridge.
GARTSHORE, I. S. 1966 *J. Fluid Mech.* **24**, 89.
KEFFER, J. F. 1965 *J. Fluid Mech.* **22**, 135.
KEFFER, J. F. 1967 *J. Fluid Mech.* **28**, 183.
MARÉCHAL, J. 1967 *C.R. Acad. Sci. Paris* A **265**, 478.
REYNOLDS, A. J. 1962 *J. Fluid Mech.* **13**, 333.
TUCKER, H. J. & REYNOLDS, A. J. 1968 *J. Fluid Mech.* **32**, 657.
TOWNSEND, A. A. 1949 *Aust. J. Sci. Res.* **2**, 451.
TOWNSEND, A. A. 1954 *Quart. J. Mech. Appl. Math.* **7**, 704.
TOWNSEND, A. A. 1976 *The Structure of Turbulent Shear Flow.* Cambridge University Press.
TOWNSEND, A. A. 1979 *J. Fluid Mech.* **95**, 515.
TOWNSEND, A. A. 1980 *J. Fluid Mech.* **81**, 171.